Residual Stresses Due to Grinding

by

Gregory V. Moeller

Thesis submitted to the Faculty of the

Virginia Polytechnic Institute and State University

in partial fulfillment of the requirements for the degree of

MASTER OF SCIENCE

in

Engineering Mechanics

APPROVED:

Prof. Norman Dowling, Chairman

Prof. Surot Thangitham

Prof. Ronald W. Landgraf

Prof. Robert W. Hendricks

July, 1995

Blacksburg, VA

Key words: Grinding, Cam, Camshaft, Mechanical Stress, Thermal Stress, Plasticity, Residual Stress

c.2

RESIDUAL STRESSES DUE TO GRINDING

by

Gregory V. Moeller

Prof. Norman Dowling, Chairman

Engineering Mechanics

ABSTRACT

An analytic treatment of stresses and temperatures generated during grinding is presented from an elasticity approach. A two dimensional heat conduction model employs an energy partition scheme in the grinding zone to produce realistic temperature profiles. By using the basic equations of thermoelasticity, the temperature profiles yield thermal stresses. An extension of the Hertzian contact theory yields mechanical stresses, which are then superimposed on the thermal stresses. Approximate plasticity corrections are used to approximate the deformation as the grinding wheel passes over the workpiece.

Subsurface results are qualitatively consistent with those found experimentally. However, they still do not agree with near-surface experimental results. Possible explanations and areas of further research are discussed.

ACKNOWLEDGMENTS

A warm thank-you goes out to the many sponsors of this comprehensive project. Without their support I would not have had this great learning experience. The sponsors include the National Science Foundation Strategic Manufacturing Initiative project #230-11-110F-108-323622-1 (sponsor number DDM-9215629), and Ford Motor Company. American Stress Technologies, Litton Automotive Services, and Presta Someflor provided support in the form of parts and services.

The technical prowess of the staff at Virginia Tech thoroughly mystified me. In addition to all of the professors whose lectures I attended, I thank the individuals who contributed greatly to this research. Among these individuals who contributed greatly, I would like to emphasize my thanks to:

- My advisor, Professor Norman E. Dowling, who's amazing ability to take mathematics to its logical extent; then deftly make characteristic assumptions to arrive at a solution will always be envied by me. His engineering skill and ability is matched by his straightforward approach to life's challenges and opportunities.
- Professor Ronald W. Landgraf, who's young spirit and warm smile contributed to my decision to attend Virginia Tech. Prof. Landgraf's eternal optimism is paralleled by great technical ability. In addition, I would like to thank Prof. Landgraf and Prof. Dowling for introducing me to the Wohler Symposium.
- Professor Robert W. Hendricks, who's enthusiastic nature towards new areas of research became an inspiration. Prof. Hendrick's is both good-hearted and technically competent. It is Prof. Hendricks' constructive criticism that I will forever keep in RAM as I continue in life.
- Professor Surot Thangitham, who's knowledge of thermal stresses was of great importance to my progress.

- Professor Adrienne Lavine for her invaluable assistance in the thermal aspects of my work.

- The other students I worked alongside during this project: Heidi Allison, Scott Courtney, Bill Cooper, Benoit Girardin, Jose Escobar, Brian Biggi, Melanie Lewis, Robin Ott, and Andy Neuman. Their contributions and insights are too great to number. An additional thanks is in order for Scott Courtney and Bill Cooper. Scott Courtney extended his warm hospitality by helping make my transition to graduate school and my new apartment a smooth one. Bill Cooper's eagerness to assist in finding information and reference materials has made my transition out of graduate school an efficient one.

My being funded by the Materials Science and Engineering Department, but studying as a student of Engineering Science and Mechanics, kept the office staff for each department in eternal limbo. For their efforts, I would like to graciously thank the staff of both the Materials Science and Engineering Department (old and new): Jan Doran, Suzette Sowers, Adele Hobday, and Amy Hill, and the Department of Engineering Mechanics: Cindy Hopkins, Pat Baker, Nancy Linkous, and Paul Sibert. Cindy Hopkins seemed to always have her finger on the pulse of the University and took extra care and time to assure day to day things went smoothly for me.

Many other people added to my colorful stay in beautiful Blacksburg, VA. I bring attention to a few outstanding individuals:

- Kate Orndorff, who's kind heart makes her the better half where ever we go as a couple. Through an unbelievable series of events, Kate and I met at Chad Binkerd's house in late July, 1993. Kate came to Virginia Tech after a short period of employment in Maryland to study Education and Learning Disabilities and will complete her studies in December, 1995.

- Chad Binkerd, who's friendship I will always treasure. The adventures I share with Chad are too great to number.

- Steve Mornelli, who I met at the graduate student orientation. Steve made sure things remained exciting and eventful in and around Blacksburg. Steve and I believe we have solved many of the world's problems during after-hours discussions.
- Brad Youngblood, who I also met at the graduate student orientation and befriended instantly. Brad's relaxed attitude and home-brewing skills help to keep things in focus in the most trying times.
- Isam Janajreh for his friendship and explanations to many technical and non-technical questions of interest to me. Isam is one of the most technically competent students I have met; I can only hope to achieve his level of competence.

Finally, the most important thank-you goes to my family. Without my mother's perseverance assuring I had the tools needed to continue the learning process, I am certain I would not have come this far. My father's love for cars inspired and enhanced my undergraduate Mechanical Engineering degree. A desire to satisfy my little brother's admiration helped me stay the course. I was assisted in plotting that course by Larry LeBlanc who is my close friend, confidant and uncle. Uncle Larry instilled his "nose-to-the-grindstone" philosophy in me and it has served me well. I thank my father's four brothers: Bob, Dade, John, and Ned, and their wives: Louise, Jeannie, Mary, and Fran. Without their career counseling, support, and financial assistance I would not have enjoyed this level of achievement.

TABLE OF CONTENTS

LIST OF FIGURES

NOMENCLATURE

Variable name	Description	Units
a_1, a_2, a_3	Lagrangian coordinates	m
α_{th}	coefficient of linear thermal expansion	1/K
β	half contact angle	radians
b	width of cam face	m
c	volumetric heat source	Watts
C_n $(n = 0, 1, ...)$	arbitrary constants, constants of integration	various
$\tilde{c}$	specific heat	Joule/kg K
$đ$	inexact differential	no units
$\delta()$	Dirac delta function.	no units
δ_{ij}	Kroneker's delta	no units
E	Young's modulus	Pascals
ε	scalar strain	mm/mm
e	nominal scalar strain	mm/mm
f_i	body force	Newtons
f_{norm}	peak normal pressure for Hertzian contact model	Pascals
F_{norm}	normal force from grinding wheel	Newtons
F_{tan}	tangential force from grinding wheel	Newtons
γ_{ijkl}	transformation tensor	Joule/kg
H	Ramberg-Osgood constant	Pascals
K	kinetic energy of R	Joules
k	thermal conductivity (except when used as a subscript)	W/m K
κ	thermal diffusivity	m^2/s
λ, μ	Lame's constants	Pascals

L_{grain}	characteristic length of an individual grain of the grinding wheel (Section 3.5)	m
L_{ij}	Lagrangian strain tensor	no units
l_{ij}	Lagrangian linear strain tensor	no units
M	moment	N/m
ν	Poisson's ratio	no units
n	strain hardening exponent (when not used as subscript)	no units
n, m, p, l	counting variables in Sections 3-4	no units
n_i	unit outward normal	no units
$P, \overline{P}$	points in R	no units
Q	heat added to R	Joules
$q(\theta)$	heat flux distribution, peak = 1.	no units
$Q, \overline{Q}$	points in R	no units
Q_0	maximum distributed heat flux	W/m^4
q_i	heat flux vector	$Watts/m^2$
ρ	mass density	kg/m^3
R	arbitrary region in space	m^3
r_{in}	inner radius of characteristic cylinder	m
r_{out}	outer radius of characteristic cylinder	m
r_{wheel}	radius of grinding wheel	m
S	arbitrary surface	m^2
σ	stress scalar	Pascals
σ_i	stress vector	Pascals
σ_{ij}	stress tensor	Pascals
t	time	sec
T	temperature	K
τ	material constant for second sound phenomenon	s

U	energy contained in R	Joules
u_i	displacement vector	m
$\tilde{u}$	energy per unit mass	Joule/kg
V	volume	m^3
v_i	velocity vector	m/s
W	work done on R	Joules
ω_{cam}	rotational velocity of wheel	rad/s
ω_{wheel}	rotational velocity of wheel	rad/s
y_1, y_2, y_3	Eulerian coordinates	m
ζ_{ij}	transformation tensor	Joule/kg

1. INTRODUCTION

"Split-second timing is essential for smooth and powerful running in a car engine. It is achieved by the engine's camshaft and crankshaft working in concert." "As the pistons move up and down in the cylinders, they drive the crankshaft which turns the flywheel and, ultimately, the wheels. But, through a chain linkage, the crankshaft also turns the camshaft. As the camshaft rotates, the cams operate the cylinder valves." - David Macauley, The Way Things Work

This thesis continues the efforts of an already well developed research project. The project focuses on more reliably predicting and extending the service life of camshafts. Once an engineer chooses cam material, profile and valve-train configuration, advances in cam service-life necessarily emerge from improved manufacturing processes. Since the final manufacturing process is usually the most influential, the effect of grinding has been the central theme of this project.

The principal investigators conceived this project with the well-founded notion that the residual stress state of the finished product influences cam service life. The investigators insightfully divided the project into logical parts. The parts included an initial literature review, experimental determination of residual stress profiles, prediction of service life given the experimental profiles, and prediction of the residual stress profiles as a result of manufacturing processes. The material contained herein pertains to the prediction of residual stress as a result of cam manufacture. The study focuses on the cams manufactured for Ford by Presta Someflor, but the information pertains to any ground cam.

1.1 CAM TERMINOLOGY, DESIGN, AND MANUFACTURE

Typically, the cam of an internal combustion engine is divided into four regions, the nose, the base circle, the opening ramp and the closing ramp (see Figure 1-1).

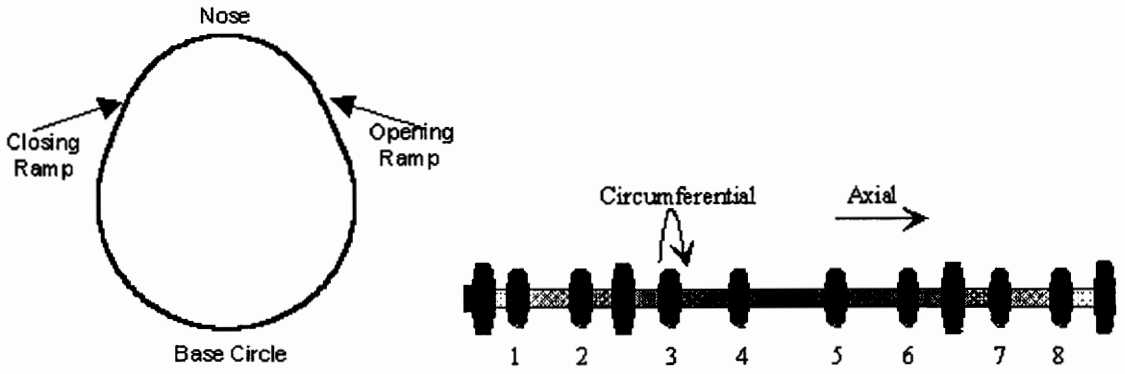

Figure 1-1 Cam lobe nomenclature. The particular Presta shafts that have been the focus of previous, supporting studies and are the focus of this study have eight lobes, numbered sequentially from left to right.

The simplest region of this type of cam is the base circle, which, by definition, is a circle with its center at the center of rotation. The base circle is a dwell period for the cam where either the exhaust and power strokes (intake lobe), or the intake and power strokes (exhaust lobe) occur. The nose is the point where the intake and exhaust ramps meet. Cam designers are caught between a "rock and a hard place" designing the ramps and nose. While it is desirable to have a period of dwell at the nose to allow gasses (fuel and air, or exhaust) to pass through, the dynamics usually dictate the cam shape. Therefore, the nose of a cam is just part of a polynomial that encompasses all three regions of the cam, the intake ramp, the nose, and the exhaust ramp. As a starting point, designers typically require that an automotive cam has a given displacement at a given angle and that the derivative of acceleration, known as jerk, is continuous.

In recent years, automobile designers at Ford moved towards roller-follower type valve-trains (see Figure 1-2) for the reduced noise, increased fuel efficiency, and increased performance.

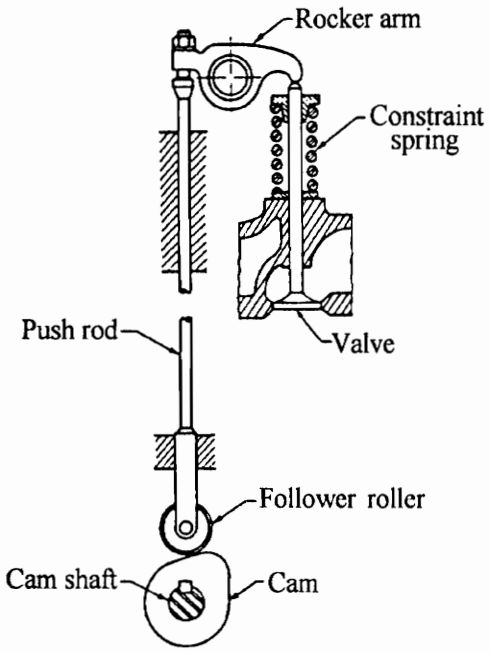

Figure 1-2 Overhead valve and roller-follower configuration

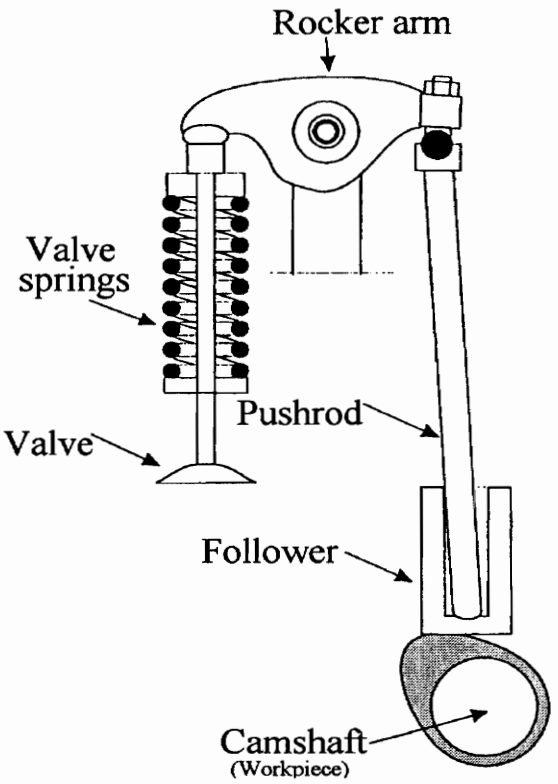

Figure 1-3 Overhead valve and flat-tappet configuration [Hugnell, n.d.]

Additionally, the roller-follower offers decreased surface wear compared to that of the flat-tappet follower (see Figure 1-3) by virtually eliminating the rubbing action of the flat tappet [See Hugnell, n.d. for a wear analysis]. However, due to the reduced contact area, a roller-follower increases service loads in otherwise similar configurations. Increased service loads translate directly to decreased service life.

To combat the increased service loads, the dynamic mass of the valve-train can be reduced by using an overhead cam configuration. This reduced dynamic mass is a consequence of the elimination of the pushrod and tappet (compare Figure 1-2 and Figure 1-4).

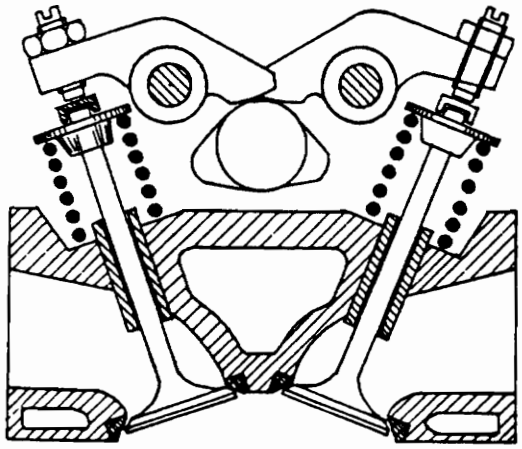

Figure 1-4 Overhead cam and roller-follower configuration

Through this sacrificial approach to valve-train design and further optimization of the remaining parts, engineers "eked" out much of the excess dynamic mass in the valve-train. For further increases in service life, attention has turned toward the manufacturing processes.

During manufacture, the camshafts manufactured by Presta Someflor go through numerous processes, including induction hardening, press fitting and grinding [Courtney, 1993, pp. 1-13]. Since the final manufacturing process generally has the most significant effect on the quality of the finished part, grinding will be the focus here. However, it should be noted that, prior to grinding, the part is induction hardened to a depth of approximately 2.5 millimeters and that the assembly forces required to press fit the lobes on the shaft are significant; both of these processes influence the state of residual stress. The significance of the processes prior to grinding is not investigated here. The lobes are assumed to be in a stress-free state before grinding.

1.2 Work Completed to Date

The accomplishments prior to this work have been significant. Scott Courtney and Marc Tricard spearheaded the initial research, creating an extensive and

comprehensive grinding data base. Courtney continued with this momentum, focusing his efforts on experimentally determining the residual stress state of the finished cam lobes. His work culminated with a thesis, cited in the bibliography herein. As Courtney was conducting research, Benoit Girardin took advantage of Courtney's seniority by absorbing as much information as possible from him. Girardin's efforts predicted the cam life as a result of the predetermined residual stress state. Girardin's efforts also produced a substantial thesis cited herein.

2. BACKGROUND

*"The sciences do not try to explain, they hardly even try to interpret, they mainly make models. By a model is meant a mathematical construct which, with the addition of certain verbal interpretations, describes observed phenomena. The justification of such a mathematical construct is solely and precisely that it is expected to work." -John von Neumann**

The following literature review includes a description of the mathematical tools used to predict residual stress herein. Section 2.1 derives the governing equations from a continuum mechanics approach using tensor notation. Section 2.2 provides a brief description of what residual stress is, how it is caused, why it is of interest, and methods of predicting it. In addition, some works cited include in-depth analysis of measurement techniques [Courtney, 1993], [Vansevenant, 1987].

2.1 Derivation of Governing Equations†

As technology is pushed further ahead, it has become necessary for scientists and engineers to revisit the assumptions inherent in the governing equations they are using. For this reason a thorough development of the governing equations is contained herein. In addition, the author has found a wealth of research areas that could have impact on grinding research. He does his best to bring attention to these areas, so subsequent researchers are aware of the knowledge base available.

It is common knowledge that coupling occurs between many processes. The thermal stress analysis presented in this paper is a quasi-static approach. Approximate plasticity corrections are implemented after the elastic stress field is calculated. This

---

* John von Neumann (1903-1957): US mathematician born in Hungary.

† The interested reader should refer to [Frederick, 1965] for a definition of terms and a more in-depth treatment.

section reviews the assumptions made when using this approach by deriving the governing equations used from basic principles

2.1.1 LAGRANGIAN LINEAR STRAIN TENSOR

The standard notion of strain is a scalar change in length. Typically when solids are analyzed a Lagrangian approach to strain (see Figure 2-1) is the method of choice, as opposed an Eulerian approach, which is more common in fluids (see Figure 2-2).

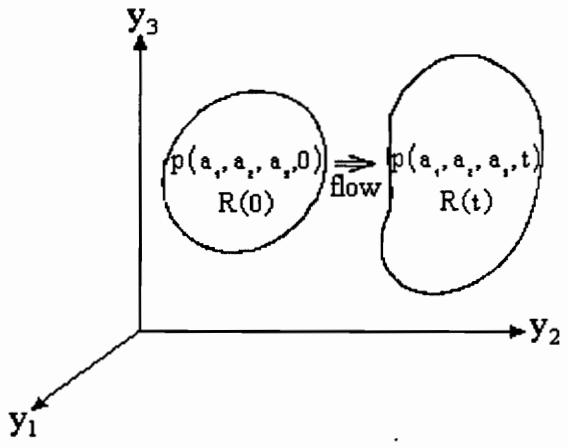

Figure 2-1 Undeformed and deformed regions using Lagrangian viewpoint [Frederick, 1965, p. 74]

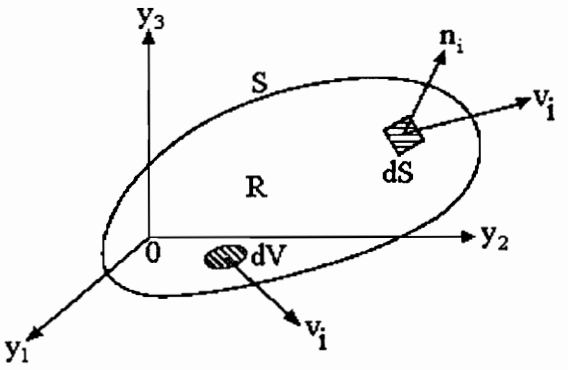

Figure 2-2 A fixed region of space through which the continuum flows, using the Eulerian viewpoint [Frederick, 1965, p. 76]

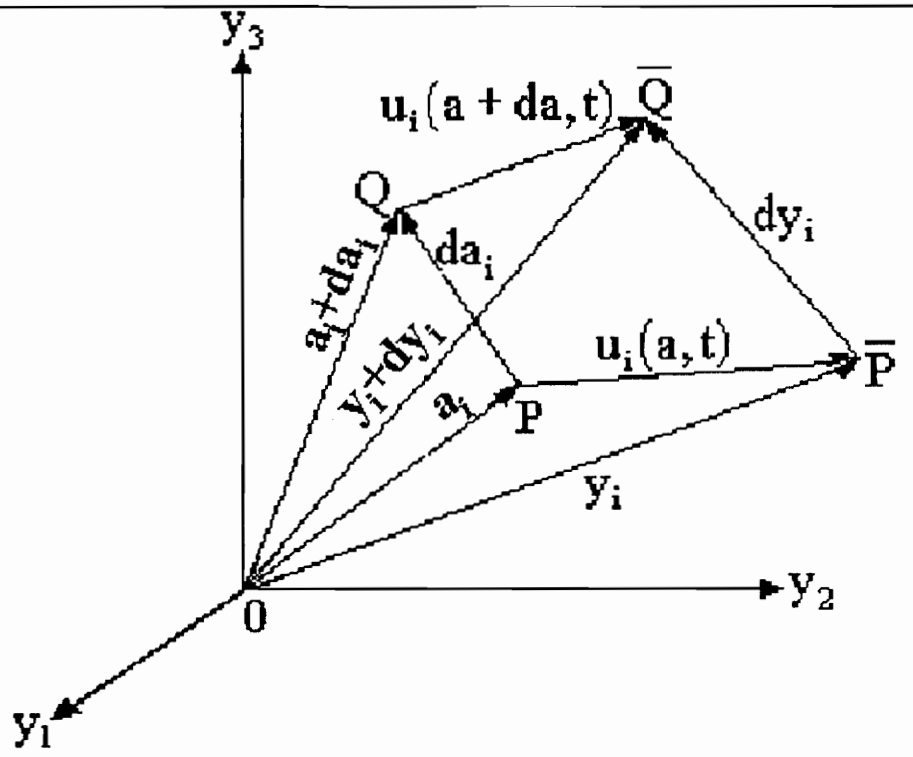

Figure 2-3 Relative displacements between two neighboring points in a continuum [Frederick, 1965, p. 80]

The deformation map in Figure 2-3 places no restrictions on displacement or rotation magnitudes. It is the difference in the magnitudes of the vectors dy_i and da_i that is of importance. We can reduce the mathematical difficulty by choosing to speak of the difference of the squares of these magnitudes.

$$\left(length \quad \overline{PQ}\right)^2 - \left(length \quad PQ\right)^2 = \left(dy\right)^2 - \left(da\right)^2 = dy_i dy_i - da_i da_i$$

At a given time, t, the vector dy_i can be expressed as:

$$dy_i = \left(\frac{\partial y_i}{\partial a_j}\right)_P da_j$$

After some manipulation, one finds the following equation for displacements valid:

$$(dy)^2-(da)^2=\left[\frac{\partial u_i}{\partial a_j}+\frac{\partial u_j}{\partial a_i}+\frac{\partial u_r}{\partial a_i}\frac{\partial u_r}{\partial a_j}\right]da_i da_j$$

It is common notation to define the strain tensor as:

$$L_{ij}=\frac{1}{2}\left[\frac{\partial u_i}{\partial a_j}+\frac{\partial u_j}{\partial a_i}+\frac{\partial u_r}{\partial a_i}\frac{\partial u_r}{\partial a_j}\right] \tag{2.1}$$

which is where the notorious factor of one-half comes from; it is part of the definition of the strain tensor. It can be seen that strain is a second order Cartesian tensor. Although a deformation scheme has been implemented to describe deformation, we have not yet limited material behavior in any way.

At this point, the first assumption is made about the material behavior. If it can be assumed that the displacement gradients are small, the third term in Equation (2.1) can be neglected since it is of second order. This assumption yields the familiar Lagrangian linear strain tensor.

$$l_{ij}=\frac{1}{2}\left[\frac{\partial u_i}{\partial a_j}+\frac{\partial u_j}{\partial a_i}\right]=\frac{1}{2}\left[u_{i,j}+u_{j,i}\right] \tag{2.2}$$

By enforcing the fact that displacements must be single-valued and continuous, we can show that the Lagrangian linear strain tensor must also satisfy the compatibility equations.

$$l_{ij,kl}+l_{kl,ij}=l_{ik,jl}+l_{jl,ik} \tag{2.3}$$

2.1.2 Reynolds' Transport Theorem

Applying the Gauss Theorem, which converts a surface integral to a volume integral, to an arbitrary material quantity, $F_{ijk...}$, and assuming our elemental mass, $\rho(y,t)dV(y,t)$, does not change, we can derive Reynolds' Transport Theorem for Lagrangian coordinates.

$$\frac{d}{dt}\int_{R(t)} \rho(y,t)F_{ij\_}(y,t)dV(t) = \int_{R(0)} \rho(a,0)\frac{dF_{ij\_}(a,t)}{dt}dV(0) = \int_{R(t)} \rho(y,t)\frac{dF_{ij\_}(y,t)}{dt}dV(t) \tag{2.4}$$

From the left side of this equation, which is the control system, to the middle equality, it is assumed that the elemental mass $\rho\, dV$ is constant. The comoving derivative using Lagrangian coordinates is expanded to get from the middle to the left equality.

2.1.3 Energy Balance

Starting with conservation of energy, we can write an energy balance:

$$\frac{đQ}{dt} + \frac{đW}{dt} = \frac{dU}{dt} + \frac{dK}{dt} \tag{2.5}$$

where we have taken time rates to make it convenient to apply Reynolds' Transport Theorem and:

$đQ$ = heat added to system. Because this term cannot be written as the comoving derivative of a thermodynamic variable, it is an inexact differential.

$đW$ = work done by surroundings on the system. This is also an inexact differential.

dU = internal energy due to thermal motions of molecules, elastic energy, etc. This is an exact differential, since it can be written as the comoving derivative of thermodynamic variables.

dK = the kinetic energy of the system. This is also an exact differential.

Looking ahead to some equations to be discussed, it is interesting to note that the heat conduction equation (2.26), the elasticity equations (2.31) and thermoelasticity equations (2.34) all come from the energy balance used to develop the first and second laws of thermodynamics (2.5). In order to point out the assumptions inherent in the governing equations used herein, it is necessary to develop them from first principles.

2.1.3.1 The Heat Term

Heat can be added to the control system in two ways. It can either pass through the boundaries as a heat flux, or be added as a volumetric heat source (i.e. internal heat generation and radiation). If a vector representing heat per unit area per unit time is defined as q_i, it can be integrated over the control surface to obtain the total heat input due to heat flux.

$$-\int_S q_i n_i \, dS \tag{2.6}$$

The negative sign is due to the unit normal, n_i, being defined as outward (see Figure 2-2). If we let c represent the volumetric heat transfer per unit time per unit mass, it can be integrated over the volume to obtain the total volumetric heat input.

$$\int_R \rho c \, dV \tag{2.7}$$

Applying the Gauss' theorem, which relates a surface integral to a volume integral, to Equation (2.6) and combining the result with Equation (2.7), the heat term becomes:

$$\frac{dQ}{dt} = -\int_R \left(q_{i,i} - \rho c\right) dV \tag{2.8}$$

2.1.3.2 The Work Term

Work can be done on the control system in two ways. A body force such as gravity can act on the body through some distance, or a stress can act on an area across the surface. Summing all of these effects, we get:

$$\frac{dW}{dt} = \int_S \sigma_i v_i \, dS + \int_R f_i v_i \rho \, dV$$

Using Cauchy's relation ($\sigma_j = \sigma_{ij} n_i$) and applying the Gauss' theorem, which relates a surface integral to a volume integral, to the first term on the right:

$$\frac{dW}{dt} = \int_R \left[\left(\sigma_{ji} v_i \right)_{,j} + \rho f_i v_i \right] dV \tag{2.9}$$

The stress tensor, σ_{ij}, includes both the conservative (elastic) and dissipative (plastic) stress fields at this point.

2.1.3.3 The Internal Energy Term

A body can also contain energy internally in many different forms; residual stress and relative motion between the atoms. The relative motion between the atoms is generally measured as temperature.

$$\frac{dU}{dt} = \frac{d}{dt} \int_R \rho \tilde{u} \, dV = \int_R \rho \frac{d\tilde{u}}{dt} dV \tag{2.10}$$

The tilde is used to distinguish the differential internal energy per unit mass, $\tilde{u}$, from displacement, u.

2.1.3.4 The Kinetic Energy Term

The net velocity of the elemental masses in the control system has an energy associated with it, which can be represented by:

$$\frac{dK}{dt} = \frac{d}{dt} \int_R \frac{1}{2} \rho v_i v_i \, dV = \int_R \rho \frac{d}{dt} \left(\frac{v^2}{2} \right) dV \tag{2.11}$$

2.1.3.5 First Law of Thermodynamics

If we combine Equations (2.5), and (2.8) to (2.11), taking into account we are integrating over an arbitrary region, the result is the first law of thermodynamics, also known as the differential energy equation.

$$\frac{d}{dt} \left(\tilde{u} + \frac{v^2}{2} \right) = \frac{1}{\rho} \left(\sigma_{ji} v_i \right)_{,j} + f_i v_i - \frac{1}{\rho} q_{i,i} + c \tag{2.12}$$

To this point, we have used the law of conservation of energy, the Gauss' theorem, and Reynolds's transport theorem. The following sections emphasize assumptions made to reduce the differential energy equation to the governing equations.

2.1.4 HEAT CONDUCTION EQUATION

This section develops the equations used for calculating temperature distributions during grinding. The assumptions made are pointed out throughout this development and summarized at the end of the section.

We can subtract the well known work-kinetic energy equation

$$-\frac{d}{dt}\left(\frac{v^2}{2}\right)=\frac{1}{\rho}\sigma_{ji},_j v_i + f v_i \qquad \textit{(work-energy equation)}$$

from Equation (2.12) to obtain another form of the First Law of Thermodynamics.

$$\frac{d\tilde{u}}{dt}=\frac{1}{\rho}\sigma_{ji}v_{i,j}-\frac{1}{\rho}q_{i,i}+c \qquad \textbf{(2.13)}$$

This is the form of the first law of thermodynamics used to derive the equations that follow.

2.1.4.1 DISSIPATIVE PROPERTIES

The stress tensor, σ_{ij}, can be separated into its conservative and dissipative parts (Equation (2.14)).

$$\sigma_{ji}=(\sigma_{\text{cons}})_{ji}+(\sigma_{\text{diss}})_{ji} \qquad \textbf{(2.14)}$$

Substituting (2.14) into (2.13), we can rewrite Equation (2.13) as:

$$\frac{d\tilde{u}}{dt}=\frac{1}{\rho}(\sigma_{\text{cons}})_{ji}v_{i,j}+\frac{1}{\rho}(\sigma_{\text{diss}})_{ji}v_{i,j}-\frac{1}{\rho}q_{i,i}+c \qquad \textbf{(2.15)}$$

which is a combination of the first and second laws of thermodynamics. In a complete plasticity analysis, Equation (2.15) would be used as is. However, the computations are greatly simplified by neglecting the dissipative stress term.

When the dissipative stress term is neglected, it should be noted that we change the nature of the heat input terms as well. This change is indicated by a subscript in Equation (2.16),

$$\frac{d\tilde{u}}{dt} = \frac{1}{\rho}(\sigma_{\text{cons}})_{ji} v_{i,j} - \frac{1}{\rho}(q_{\text{cons}})_{i,i} + c_{\text{cons}}, \tag{2.16}$$

where $(\sigma_{\text{diss}})_{ji} = 0$

which is referred to as the entropic equation of state. Neglecting the dissipative terms possibly causes the contradiction between Fourier's Law and the entropic equation of state alluded to later in Section 2.1.4.5.

Furthermore, by neglecting the dissipative term, we are losing the term which accounts for plastic deformation of the material. Consequently, if no residual stress was present before a reversible process occurred, no residual stress will be present after the process occurred. This is addressed in Section 2.2.2.

2.1.4.2 INTERNAL ENERGY TERM

If we assume the internal energy term from (2.16) to be a function of the Lagrangian linear strain tensor as developed in Section 2.1.1, and temperature, we can write:

$$d\tilde{u}(l_{ij}, T) = \frac{\partial \tilde{u}}{\partial l_{ij}} dl_{ij} + \frac{\partial \tilde{u}}{\partial T} dT \tag{2.17}$$

$$\text{where } \tilde{c} = \frac{\partial \tilde{u}}{\partial T}$$

If it is assumed that the material is both isotropic and homogeneous (this is addressed in Section 2.1.5) and the process is reversible, the first term on the right hand

side of Equation (2.17) the following equality holds true [Frederick, 1965, pp. 167 - 169]:

$$\frac{\partial \tilde{u}}{\partial l_{ij}} = \frac{1}{\rho}\left[(\sigma_{cons})_{ji} - (3\lambda + 2\mu)\alpha_{th}\delta_{ij}T\right] \tag{2.18}$$

Even if the process is reversible there is a term which stems from the derivation of (2.18) that is assumed to be zero (2.19) [Frederick, 1965, p. 168, equation 5.137 to 5.138]. This is, in fact, another research area.

$$\frac{\partial\left(\frac{1}{T}\right)}{\partial l_{ij}} = 0 \qquad \textit{(assumed)} \tag{2.19}$$

However, in light of our other assumptions, this term can surely be neglected in our analysis.

2.1.4.3 The Stress and Velocity Gradient Product

The velocity gradient can be conveniently expressed in terms of the strain tensor by using the property of symmetry possessed by the strain tensor.

$$v_{i,j} = \left(\frac{\partial u(l_{ij})}{\partial t}\right)_{,j} = \frac{\partial\left[\frac{1}{2}\left(u_{i,j} + u_{j,i}\right)\right]}{\partial t} = \frac{\partial(l_{ij})}{\partial t} \tag{2.20}$$

2.1.4.4 HEAT FLUX TERM

In 1808 Fourier* proposed a model governing the transfer of heat energy. It became known as Fourier law of heat conduction. The Fourier law of heat conduction says that the rate of heat flow through a substance is proportional to the area normal to the direction of flow and negative to the rate of change of temperature with distance along the direction of flow [Parker, 1994, p. 797].

$$q_i = kT_{,i} \tag{2.21}$$

Notice the law does not specify q for a reversible process, which could give rise to the "second sound" phenomenon mentioned later in Section 2.1.4.5.

In using Fourier's law it is assumed the material conductivity is not directional, i.e. the material is assumed isotropic. Fourier's law was later generalized by Duhamel in 1838 to include anisotropic heat conduction. Although all materials exhibit anisotropic properties to some extent, this is not addressed in this study.

2.1.4.5 SECOND SOUND PHENOMENON

Heat must propagate at a finite speed. Therefore, it is contradictory to use both the equation of state (2.17) and Fourier's Law (2.21). This contradiction was first noted by Maxwell† in 1867 [Maxwell, 1867], and has been a topic of research [Szekeres, 1980], [Farkas, 1983], [Tarkenton, 1994], [Chandrasekharaiah, 1986]. The modified equation of state used has been proposed in the form [Szekeres, 1980]:

$$du\left(l_{ij}, T, \dot{T}\right) = \frac{\partial u}{\partial l_{ij}} dl_{ij} + \frac{\partial u}{\partial T} dT + \frac{\partial u}{\partial \dot{T}} d\dot{T}, \qquad \text{where } \frac{\partial u}{\partial \dot{T}} = \tilde{c}\tau \tag{2.22}$$

An alternative formulation associating the "second sound" phenomenon with the heat flux vector was also proposed in the form:

---

* Jean Baptiste Joseph Fourier (1768-1830): French mathematician and physicist.

† James Clark Maxwell (1831-1879): Scottish physicist.

$$\tilde{\tau}\dot{q}_i + q_i = kT_{,i} \tag{2.23}$$

This gives rise to a hyperbolic equation of heat conduction, giving a finite speed of heat propagation. Experimental results have suggested the material constant τ could have values between 10^3 s and 10^8 s. In very fast heating or cooling applications, such as internal combustion engines, this could effect thermal stresses as much as 8% [Farkas, 1983, p. 164]. In this analysis, it will be assumed that the process is sufficiently slow to neglect the time dependence of temperature propagation known as the "second sound" phenomenon.

2.1.4.6 Radiative Term

If one were to put two bodies of different temperature in a vacuum, surely heat could not be transferred by conduction or convection. However, it would be found that there is a transfer of heat energy from the body of higher temperature to the body of lower temperature. All surfaces of finite temperature emit energy in the form of electromagnetic waves [De Witt, 1990]. The last term on the right hand side of the differential energy equation is considered to account for radiative energy. It has been determined that energy losses due to radiative effects during grinding are negligible in comparison to those due to conduction and convection [Egshy, 1967], so that:

$$c \cong 0 \tag{2.24}$$

If heat loss due to radiation needs to be accounted for, an equivalent convective heat transfer rate can be used to account for these losses. This quantity has been determined to be about $30\frac{Joules}{m^2 s \cdot K}$ given an average temperature of $480^{o}C$ [Vansevenant, 1987, p. 3-25].

2.1.4.7 Heat Conduction Equation

If Equations (2.13)-(2.24) are combined, the result is the coupled heat conduction equation of linear thermoelasticity (2.25).

$$kT_{,ii} = \rho\tilde{c}\frac{\partial T}{\partial t} + (3\lambda + 2\mu)\alpha_{th}T\frac{\partial (l_{ii})}{\partial t} \tag{2.25}$$

However, the coupling term which relates the rate of cubical dilatation to temperature will not be considered here.

To summarize, the material investigated is assumed to have both isotropic and homogeneous properties with respect to the stress-strain relations. It is assumed to be isotropic with respect to the heat conduction coefficient. The process is assumed to be reversible. We are neglecting the second sound phenomenon and coupling between cubical dilatation and temperature. We have now reduced the first law of thermodynamics to the uncoupled heat conduction equation (2.26).

$$T_{,ii} = \frac{\rho\tilde{c}}{k}\frac{\partial T}{\partial t} \tag{2.26}$$

In general, the material constants, $k, \rho, \tilde{c}$, are temperature dependent (see Figure 2-17).

2.1.5 Mechanical Stress Equations

This section develops the equations used for elastic stress calculations due to surface traction during grinding. Attention is brought to assumptions made during the development, which are summarized at the end of the section. Previous models developed by other scientists are used as part of our later analysis and are briefly explained in Section 2.1.5.3.

2.1.5.1 Generalized Hooke's Law

If the assumptions inherent in (2.16) are made, the heat transfer terms are neglected, and the velocity term is expressed in terms of the linear strain tensor as in (2.20), we can write:

$$d\tilde{u}(l_{ij}) = \frac{1}{\rho}(\sigma_{cons})_{ij}\, dl_{ij} \tag{2.27}$$

If $\tilde{u}$ is expanded in a power series, we get:

$$\tilde{u} = C_0 + \zeta_{ij} l_{ij} + \gamma_{ijkl} l_{ij} l_{kl} + \ldots\ldots \tag{2.28}$$

where C_0 represents initial displacement and ζ_{ij} represents residual stress. If the initial displacement and residual stress are zero, strain energy begins with the third term. Higher order terms, which represent non-linear, elastic stress-strain relationships, are yet another area of research.

Considering the symmetric properties of the stress and strain tensors, it can be shown that:

$$\tilde{u} = \frac{1}{2} \gamma_{ijkl} l_{ij} l_{kl} \tag{2.29}$$

and stress is related to strain by:

$$(\sigma_{cons})_{ij} (l_{ij}) = \gamma_{ijkl} l_{kl}$$

Therefore:

$$\tilde{u} = \frac{1}{2} (\sigma_{cons})_{ij} l_{ij}$$

Also, considering the compatibility equations for strain (2.3), and the symmetry property of both the stress and strain tensors, it can be shown that there are at most 21 independent elastic constants contained in γ_{ijkl} [Frederick, 1965, pp. 148, 158].

It is interesting to point out that stress is a physical quantity that must exist since it came from the two fundamental laws of nature. However, note the method used to map deformation due to stress, i.e. strain, is an arbitrary choice.

2.1.5.2 LAME'S CONSTANTS

If we assume isotropy and homogeneity of the elastic properties (2.30), there are only two independent elastic constants relating stress and strain(2.31).

$$\gamma_{ijkl} = \gamma'_{ijkl} \quad \text{(for isotropy)} \tag{2.30}$$

where the prime indicates a rotated coordinate system

$$\gamma_{ijkl,m} = 0 \quad \text{(for homogeneity)}$$

$$(\sigma_{cons})_{ij}(l_{ij}) = \lambda l_{ii}\delta_{ij} + 2\mu l_{ij} \tag{2.31}$$

where μ and λ are Lame's constants:

$$\mu = \frac{1}{2}(\gamma_{1111} - \gamma_{1122})$$

$$\lambda = \gamma_{1111}$$

μ is also known as the shear modulus

Lame's constants are related to Young's modulus and Poisson's ratio as shown in Equation (2.32).

$$E = \frac{\mu(3\lambda + 2\mu)}{\lambda + \mu} \quad \text{Young's Modulus} \tag{2.32}$$

$$\nu = \frac{\lambda}{2(\lambda + \mu)} \quad \text{Poisson's Ratio}$$

Young's Modulus, E, is defined as the ratio of a simple tension stress applied to a material to the resulting parallel strain to the tension [Parker, 1994]. Within small temperature ranges Young's modulus is assumed constant. However, over broad temperature ranges Young's modulus is inversely proportional to temperature for most steels as can be seen for SAE 52100 (see Figure 2-14).

Poisson's ratio is the ratio of the transverse contracting strain to the elongation strain when a rod is stretched by forces which are applied at its ends and which are parallel to the rod's axis [Parker, 1994]. Although the effect of the modest change in

Poisson's ratio with respect to temperature will not be investigated here, it is provided for reference (see Figure 2-13).

To summarize, the material investigated is assumed to have both isotropic and homogeneous properties with respect to the stress-strain relations. Furthermore, the material properties are assumed to be independent of temperature. The process is assumed to be reversible. We are neglecting the second sound phenomenon, the temperature equation and its coupling term. The displacement gradients are assumed small. We have now reduced the first law of thermodynamics to the equations of elasticity (2.31).

2.1.5.3 Mechanical Pressure Models

The stress due to curved bodies in contact was first studied by Hertz* [Hertz, 1881]. His theory is based on an elastic analysis (2.31). The theory considers normal pressure only. A solution is obtained by assuming a shape for the pressure distribution that is a function of the bodies' geometry.

* Heinrich Rudolf Hertz (1857-1894): German physicist.

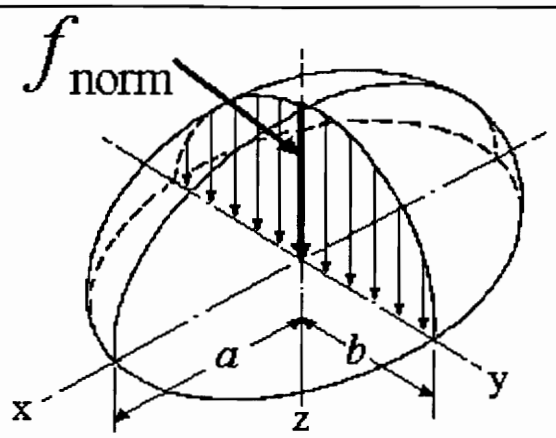

Figure 2-4 Assumed normal pressure distribution between two curved bodies in contact [Adapted from Juvinall, 1967]

Hertz's theory has been extended to include both normal and tangential forces between two cylinders in contact [Smith, 1953]. It has also been used extensively in grinding length contact models [Lindsay, n.d.], [Lindsay, 1967], [Verkerk, 1975], [Brown, 1971].

2.1.6 THERMAL STRESS EQUATIONS

This section develops the equations used for thermoelastic stress calculations due to the surface heat flux during grinding. Attention is brought to assumptions made during the development, which are summarized at the end of the section. Previous models developed by other scientists are alluded to.

Since we have already made the assumption of small displacement gradients in using the linear strain tensor we can rearrange (2.27), and write:

$$\frac{d\tilde{u}}{dl_{ij}} = \frac{1}{\rho}(\sigma_{cons})_{ij} \tag{2.33}$$

Considering (2.18), (2.31), (2.33), we can write the relationship for linear thermoelasticity (2.34).

$$(\sigma_{cons})_{ij} = \lambda I_{ii}\delta_{ij} + 2\mu I_{ij} - (3\lambda + 2\mu)\alpha_{th}\delta_{ij}(T - T_{ref}) \tag{2.34}$$

where T_{ref} is a reference temperature.

When using (2.34), the material is assumed to have both isotropic and homogeneous properties with respect to the stress-strain relations. It is assumed to be isotropic with respect to the coefficient of heat conduction. The process is assumed to be reversible. We are neglecting the second sound phenomenon, temperature equation and its coupling term. The displacement gradients are assumed small. We have now reduced the first law of thermodynamics to the equations of thermoelasticity (2.31).

2.1.6.1 Thermal Stress Models

Although the existence of the governing equations of thermoelasticity has been known for quite some time, it seems that the specifics were not sorted out completely, or at least published comprehensively, until the 1950's [Truesdell, 1984]. The study of thermal stresses was accelerated mainly as a result of research in aerodynamics [Brahtz, 1955], and was subsequently extended to grinding [El-Helieby, 1980], [Snoeys, 1972], [Skalli, 1982].

2.2 Review of Residual Stress

Stress is defined as the force acting across a unit area in a solid material resisting the separation, compacting or sliding [Parker, 1994]. Residual stress is defined as a stress system within a solid that is not dependent on external forces [Parker, 1994], [Dowling, 1993]. Residual stresses occur when a body is subject to non-uniform plastic deformation or changes in specific volume (see Figure 2-5).

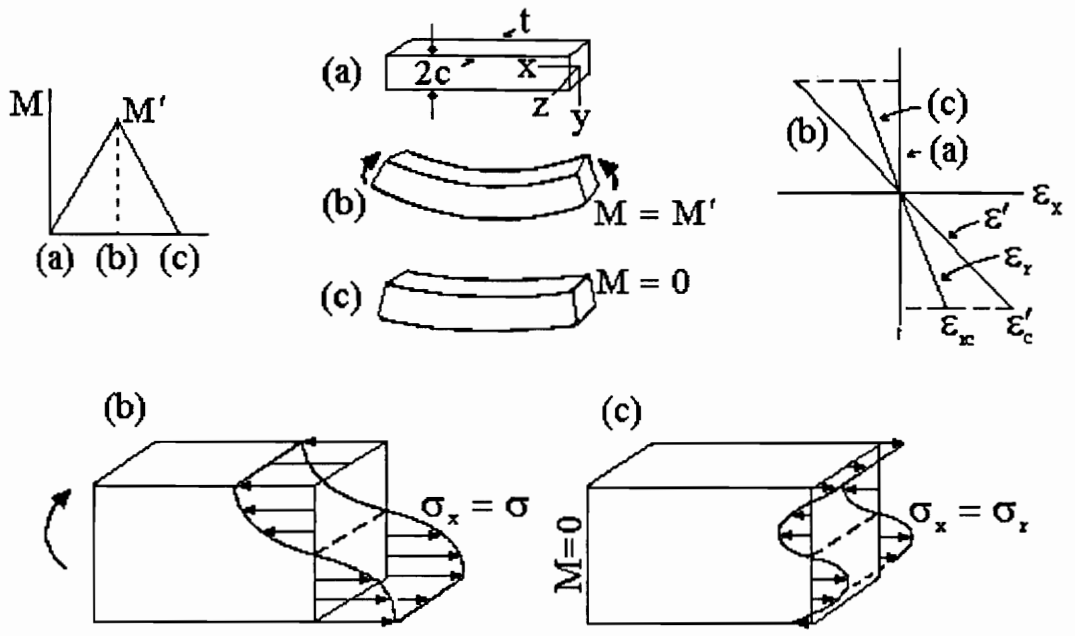

Figure 2-5 Loading of a rectangular beam beyond the point of yielding followed by unloading. Loading starts from zero moment at time (a) and proceeds to the maximum moment *M'* at time (b). When unloading is complete at time (c), residual strains ε_{res} having a linear distribution remain, and residual stresses σ_{res} are distributed as shown. [Dowling, 1993, p. 585]

A near surface compressive residual stress is desirable as it has been shown to increase the service life of parts subjected to cyclic loading [Girardin, 1994], [El-Helieby, 1980], [Landgraf, 1988] as long as subsequent yielding during service life does not adversely affect the residual stress field [Dowling, 1993, p. 434-437]. Conversely, tensile residual stresses on the surface have been shown to decrease service life by promoting crack growth [Flavenot, 1986].

Many methods have been developed to produce compressive residual stress including shot peening, cold rolling, carburizing, nitriding, and rapid quenching to name a few. The surface residual stresses investigated here are imparted by yielding. Grinding has been determined to impart either compressive or tensile residual stress depending on the severity of the grinding process [Courtney, 1993] [Vansevenant, 1987].

It is the goal of this study to predict the residual stress in camshafts. Since the final manufacturing process is grinding, this process is the focus of this study. However, it should be noted that this is not the only process in manufacturing of the cam lobes studied [Courtney, 1993, pp. 1-8]. Residual stresses induced by grinding are a difficult quantity to predict due to the temperature dependent nature of material properties, phase transformations of both the grinding fluid and possibly workpiece itself, complex stress fields (mechanical and thermal), and the highly plastic nature of the work piece deformation.

Residual stresses can exist across several orders of magnitude of scale. They can encompass the entire workpiece, or exist at the atomic scale. Residual stress has been grouped in three different categories [Vansevenant, 1987]:

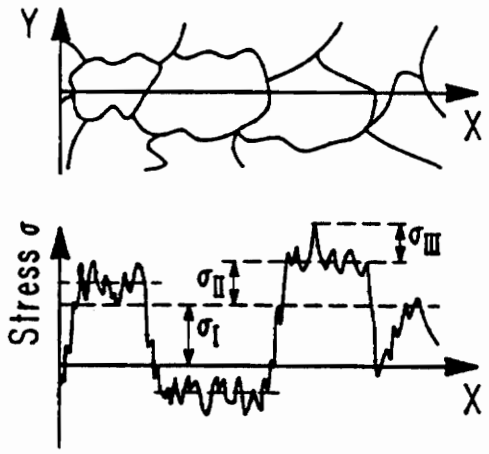

Figure 2-6 Residual stress types [Vansevenant, 1987, p. 1-2]

Type I stresses (σ_I, see Figure 2-6) are macroscopic stresses produced over the entire workpiece. They vary smoothly on scales much larger than the grain size and are continuous across the entire workpiece. They can be caused when thermal gradients or mechanical pressures are significant enough that the stresses developed exceed the yield

strength of the material. Type I stresses are typically the dominant stress in the previously described processes.

Type II stresses (σ_{II}, Figure 2-6) are homogeneous over one grain. They vary from one grain to another. Stresses of this type are caused by different thermal expansion coefficients between grains. The different coefficients of expansion are a result of different phases of the material existing in the same region or the material being poly-crystalline.

Type III stresses (σ_{III}, Figure 2-6) are non-homogeneous at the smallest scales. These stresses are the result of defects within the crystal lattice itself. These stresses are studied by scientists concerned with dislocations. Defects are commonly classified as point defects, or as screw, or edge dislocations [Flinn, 1990].

At this point, the goal of this study can be further refined. The particular stresses of interest are type I stresses. Therefore, the camshaft material will be treated as a continuum.

2.2.1 Material Behavior

In order to study material behavior past the point of yielding, one needs to know how it behaves, since the linear relationship used in elasticity theory can no longer be applied. Yielding is generally defined as 0.2% unrecoverable, or plastic, strain. These relationships can be found experimentally using testing equipment, or can be approximated by mathematical functions fitted to previously gathered data. Most steels exhibit a yield strength that is inversely proportional to temperature. Yield strength versus temperature for SAE 52100 steel can be seen in Figure 2-16.

2.2.1.1 Stress strain relationships

Scientists developed many schemes to characterize material behavior. The simplest model, elastic-perfectly plastic, characterizes loading as being fully recoverable

all the way up to the yield. Upon yielding, any further loading will result in large plastic deformations (Figure 2-7).

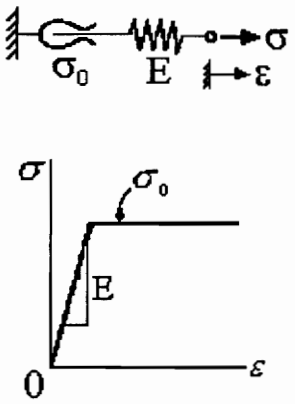

Figure 2-7 Elastic-perfectly plastic material behavior [Dowling, 1993, p. 529]

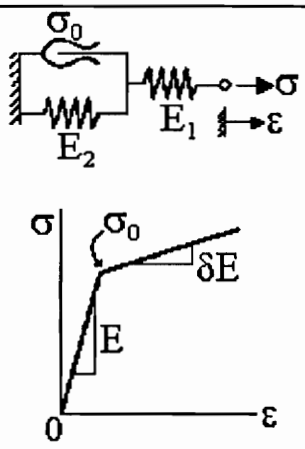

Figure 2-8 Elastic-linear hardening material behavior [Dowling, 1993, p. 529]

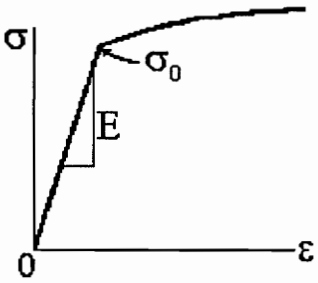

Figure 2-9 Elastic-power hardening material behavior [Dowling, 1993, p. 529]

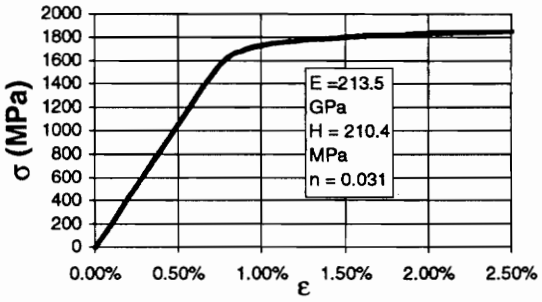

Figure 2-10 Ramberg-Osgood relationship for SAE 52100 steel

However, experimental testing of most metals shows a modest non-linear hardening response beyond yielding. As an approximation, this hardening response is sometimes characterized as linear behavior (see Figure 2-8), or as an exponential relationship (see Figure 2-9).

The models mentioned so far characterize the onset of yield as a specific event. This is not seen in real material behavior. In a report published in 1943, two scientists, Ramberg and Osgood, proposed a relationship that combined the elastic, non-linear hardening, and non-specific onset of yield in one mathematical equation (see Figure 2-10), (2.35).

$$\varepsilon(\sigma) = \underbrace{\frac{\sigma}{E}}_{elastic} + \underbrace{\left(\frac{\sigma}{H}\right)^{1/n}}_{plastic} \tag{2.35}$$

This relationship is different than previous ones in two ways. First, it predicts some plastic deformation upon any loading. Second, strain is proposed as a function of stress, rather than vice-versa. The material studied herein will be characterized by the Ramberg-Osgood relationship.

2.2.1.2 KINEMATIC HARDENING

Upon unloading, real, metallic materials exhibit a memory effect. That is, a material seems to "know" it has previously yielded and yields when $\Delta\sigma = 2\sigma'$, where σ' is the highest stress reached prior to unloading. The unloading behavior can be determined experimentally [Dowling, 1993, pp. 139-176], or can be inferred by the behavior during loading.

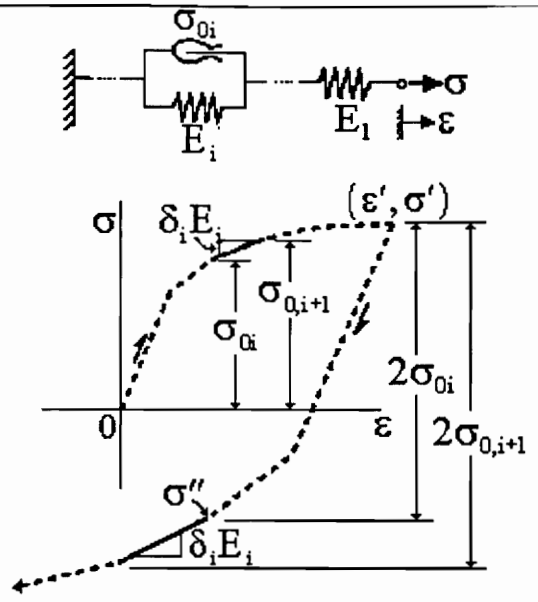

Figure 2-11 Spring-slider rheological model showing $\Delta\sigma = 2\sigma_0$ [Dowling, 1993, p. 546]

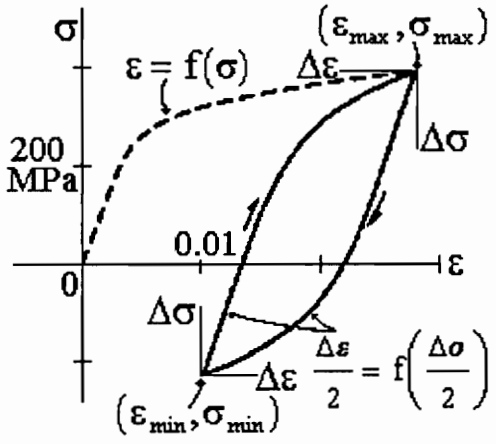

Figure 2-12 Ramberg-Osgood stress-strain behavior using kinematic hardening rule [Dowling, 1993, p. 549]

Rheological models using springs, sliders, and dashpots have been developed to better explain the mechanisms during yielding and unloading. Kinematic hardening best characterizes the non-time-dependent unloading and reloading behavior of metallic materials. It predicts that upon unloading, a material will unload elastically until $\sigma' - \sigma = 2\sigma_0$ at which point the response will follow the next stage of the initial loading slope for twice its previous length, and so on (see Figure 2-11, and Figure 2-12).

2.2.1.3 Temperature Dependent Material Properties

When changes in temperature become significant, material properties can no longer be considered constant with respect to temperature. Poisson's ratio changes approximately 10% over the temperature range of interest (see Figure 2-13). SAE 52100 steel exhibits a stiffness decrease with respect to temperature (see Figure 2-14), an increasing coefficient of thermal expansion (see Figure 2-15), and decreasing yield strength (see Figure 2-16).

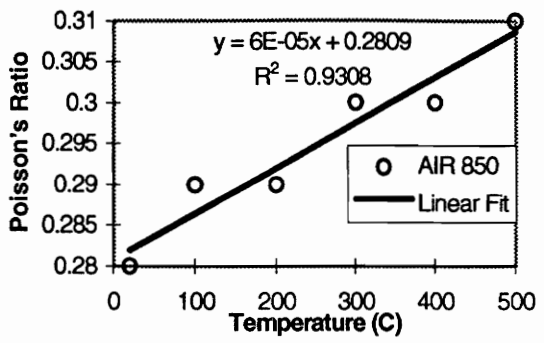

Figure 2-13 Temperature dependence of Poisson's ratio [Vansevenant, 1987, p. A-15]

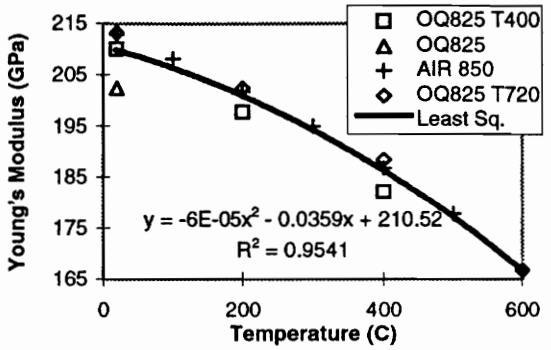

Figure 2-14 Temperature dependence of Young's Modulus [Vansevenant, 1987, p. A-12]

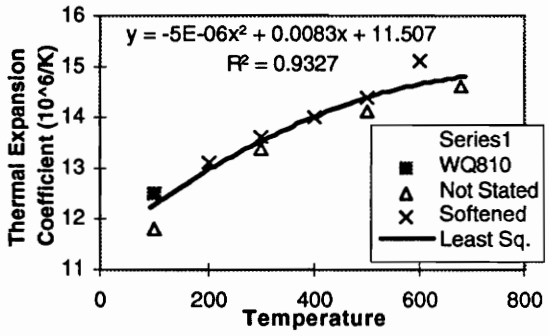

Figure 2-15 Temperature dependence of thermal expansion coefficient [Vansevenant, 1987, p. A-11]

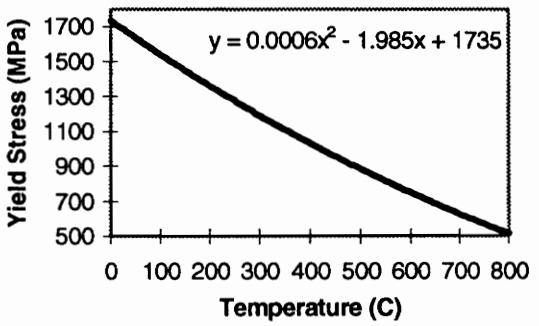

Figure 2-16 Temperature dependence of yield strength [Vansevenant, 1987, p. A-8]

These temperature dependencies affect stress calculations. They will not be treated in the stress analysis, but will be considered in the plasticity corrections.

SAE 52100 steel also exhibits temperature dependent properties that will affect the temperature calculations. The density, specific heat and thermal conductivity are all temperature dependent, and can be grouped in one constant, κ, called the thermal diffusivity (see Figure 2-17).

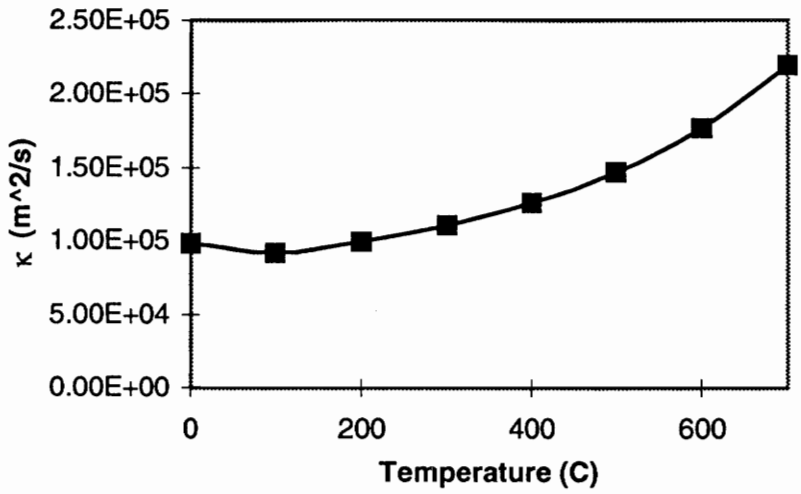

Figure 2-17 Temperature dependence of material properties $\kappa = \frac{\rho\tilde{c}}{k}$

However, this temperature dependence will not be considered in this analysis..

2.2.2 Plasticity Approximations

By dropping the dissipative stress term to simplify Equation (2.15), we have left out the term that is of interest in residual stress calculations. The result of any stress calculations will yield zero residual stress since all deformations will be reversible, or "elastic." Fortunately, correction methods have been developed to approximate the magnitude of plastic deformation in the cases of uniaxial and biaxial loading [Dowling, 1993, p. 536, 540, 590]. However, the tensor nature of the dissipative stress term is lost, so we cannot track the directionality of the residual stress.

One of the most widely used corrections methods is "so called" the Neuber's rule [Dowling, 1993, p. 598]. For nominal elasticity but local yielding, it states that the local stress times the local strain at a notch is equal to a constant (2.36). This parabola is then extended to intersect the stress-strain curve that characterizes the material response (see

Figure 2-18), which can be a real stress-strain curve or one of those described in Section 2.2.1.

$$\sigma = f(\varepsilon): \text{ stress strain curve} \tag{2.36}$$

$$k_\sigma = \frac{\sigma}{S}, \qquad k_\varepsilon = \frac{\varepsilon}{e},$$

Neuber's rule: $k_t = \sqrt{k_\sigma k_\varepsilon}$

where S is the nominal stress, E is Young's modulus, e is the nominal strain, σ is local stress and ε is local strain.

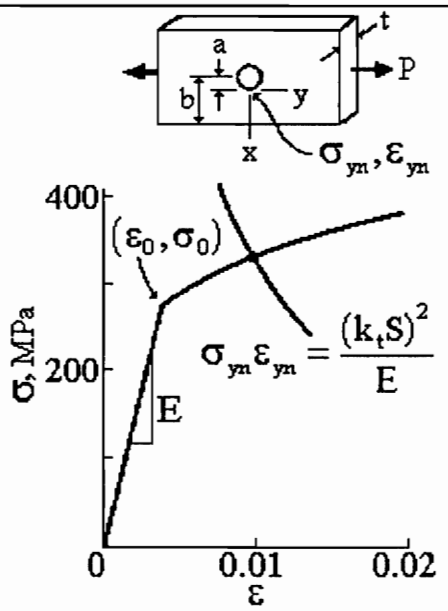

Figure 2-18 Depiction of Neuber's rule for gross plasticity correction[Dowling, 1993, p. 599]

However, Neuber's rule tends to overestimate the magnitude of the plastic deformation because redistribution of stress during loading is not accounted for (see Figure 2-19) [Glinka, 1985, p. 840]. Furthermore, Neuber's rule is typically applied at the surface of the work piece and not in-depth.

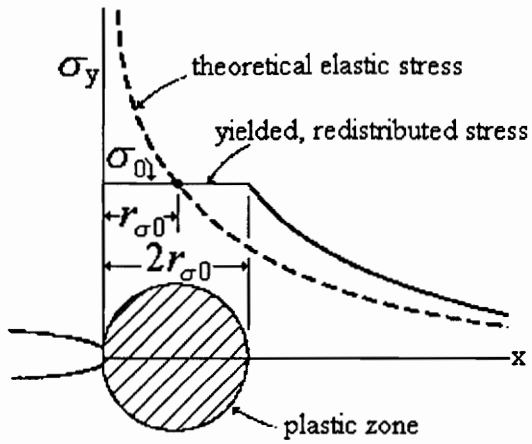

Figure 2-19 Depiction of plastic zone, showing approximate redistribution of stress [Dowling, 1993, p. 316]

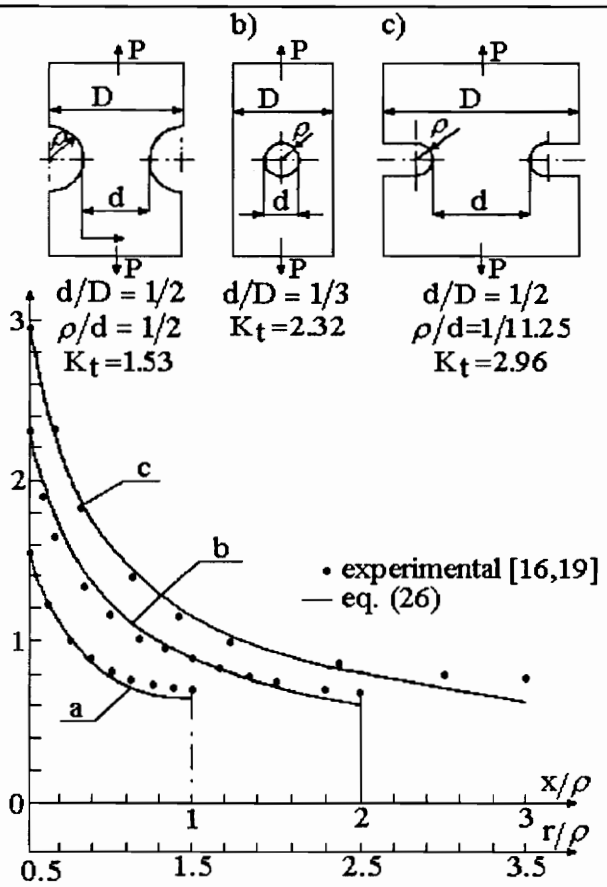

Figure 2-20 Calculated and experimental elastic stress distribution near notches [Glinka, 1985, p. 845]

G. Glinka has attempted to approximate the size of the plastic zone at a crack using the strain energy density approach. He has further extended the strain energy density approach to yield surprisingly accurate in-depth stress profiles (see Figure 2-20) [Glinka, 1985].

Although this analysis is definitely not of a crack tip, or even a notch, some method for the redistribution of stress due to yielding must be implemented. As a starting point the method of Irwin (see Figure 2-19) will be used.

3. ANALYTIC TEMPERATURE PROFILES

"Energy in natural systems exists on two levels: the macroscales, where everyday objects can be counted and measured, and the microscales, where countless atoms swim in random motion, unmeasureable except for an average entity, temperature." - James Gleick, Chaos

For this analysis the complicated geometry of the cam lobe has been reduced to a cylinder. The radius of the cylinder is equal to the local radius of the camshaft at the point of interest (see Figure 3-1).

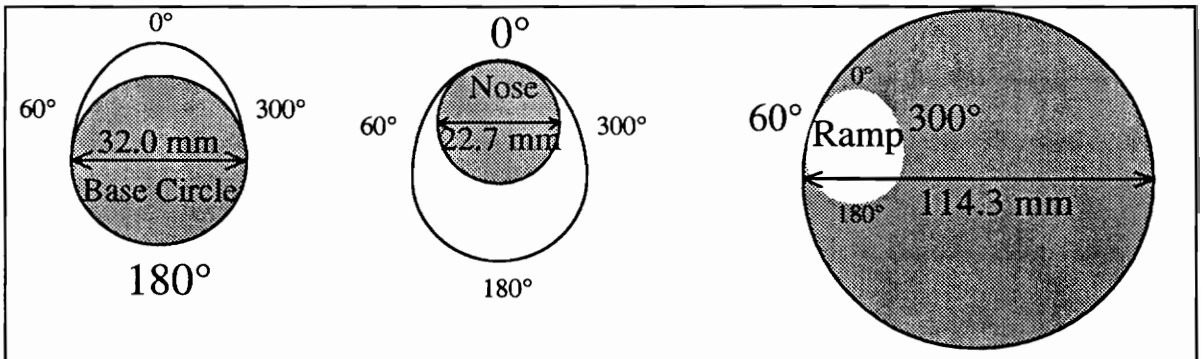

Figure 3-1 Depiction of cylinders representing local radius of curvature. The camshaft profile is in white and the characteristic cylinder in gray. [Biggi, 1995]

If the effect of varying radius of curvature proves to be small, this method will have considerable impact on all grinding processes. The design process of ground parts will become parametric as design engineers will be able to consider the effects of the manufacturing process. From fatigue models developed, they will be able to calculate service life as well [Girardin, 1994].

By extending the cylinder concept depicted in Figure 3-1, we can develop temperature profiles throughout the cylindrical body. This extension is valid because we are not interested in the temperature field throughout the workpiece. We are only

interested in temperatures very near the grinding zone where the influence of the surrounding material is assumed negligible.

3.1 THERMAL MODEL

Research specific to the thermal aspects of grinding is extensive. Snoeys (1978) and Malkin (1984) compiled literature reviews. A classic model for moving heat sources was developed by Jaeger (1942) and has been subsequently extended [Hetnarski, 1969], [Takeuti, 1980], [Lavine, 1991], [Takeuti, 1986]. The solution of interest is that of an arbitrary heat flux rotating about the surface of a cylinder with convection on the inner and outer surfaces (see Figure 3-2 and Figure 3-3).

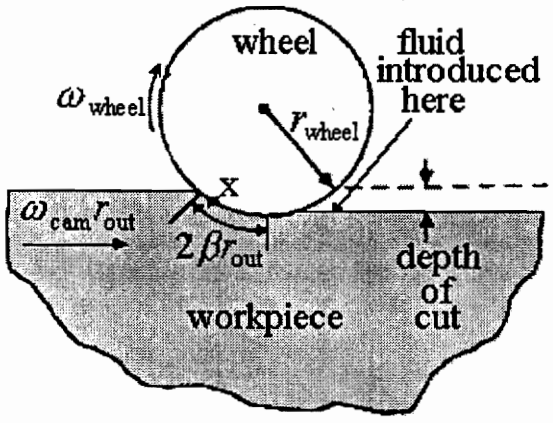

Figure 3-2 The grinding geometry

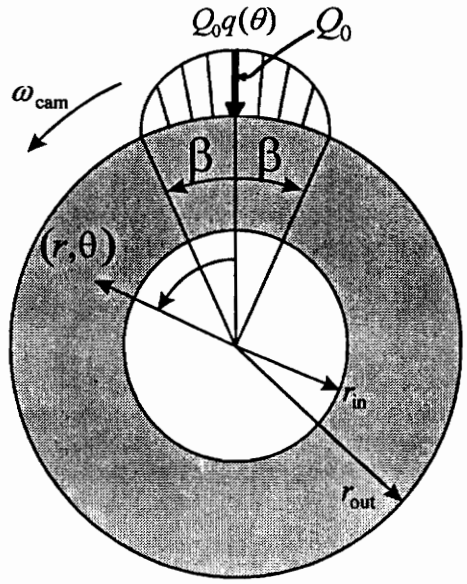

Figure 3-3 Cylinder with moving arbitrary heat flux on outer surface subjected to convection on the inner and outer surfaces

This model assumes constant, albeit different, convective heat transfer coefficients on the outer and inner surfaces. This type of analysis is very versatile in "what if" situations, (e.g., What if the inside of the cylinder had a cooling fluid running through it?). However, it fails to model the increased convective heat transfer in the grinding zone. This inconsistency can be eliminated by replacing the real power input to the wheel (surface heat flux) by a reduced power input using an energy partition. The energy partition is discussed in Section 3.5.

3.2 GOVERNING EQUATION AND BOUNDARY CONDITIONS

Making all of the assumptions needed to develop the uncoupled heat conduction equation (2.26) and implementing it for the specific case of cylindrical coordinates, we can mathematically pose the problem in Figure 3-3 as:

Non-Dimensionalized Variables: (3.1)

$$\bar{T} = kT/Q_0 r_{out}, \quad \bar{h}_{in} = h_{in} r_{out}/k, \quad \bar{h}_{out} = h_{out} r_{out}/k$$
$$\bar{r} = r/r_{out}, \quad \bar{r}_{in} = r_{in}/r_{out}, \quad \bar{t} = \kappa t / r_{out}^2$$
$$\bar{\omega} = \omega_{cam} r_{out}^2/\kappa$$

where k is thermal conductivity, h is the convective heat transfer coefficient, k is thermal diffusivity, t is time, and the rest of the variables are defined in Figure 3-3. Throughout this development, a bar denotes non-dimensional variables.

Governing Equation: (3.2)

$$\bar{T}(\bar{r},\theta,\bar{t})_{,\bar{r}\bar{r}} + \frac{1}{\bar{r}}\bar{T}(\bar{r},\theta,\bar{t})_{,\bar{r}} + \frac{1}{\bar{r}^2}\bar{T}(\bar{r},\theta,\bar{t})_{,\theta\theta} = \bar{T}(\bar{r},\theta,\bar{t})_{,\bar{t}}$$

Boundary and Initial Conditions: (3.3)

$$\bar{T}(1,\theta,\bar{t})_{,\bar{r}} + \bar{h}_{out}\bar{T}(1,\theta,\bar{t}) = 0$$

$$\bar{T}(\bar{r}_{in},\theta,\bar{t})_{,\bar{r}} + \bar{h}_{in}\bar{T}(\bar{r}_{in},\theta,\bar{t}) = 0 \quad (3.4)$$

$$\bar{T}(\bar{r},\theta,0) = \frac{\delta(\bar{r}-1)q(\theta)}{\bar{r}} \quad (3.5)$$

where $\delta(\,)$ is the Dirac delta function and $q(\theta)$ is represented by the Fourier series:

$$q(\theta) = \sum_{n=0}^{\infty} (A_n \cos n\theta + B_n \sin n\theta)$$

$$q(\theta) = \begin{cases} q(\theta) & for \quad (-\beta \le 0 \le \beta) \\ 0 & for \quad other\ \theta \end{cases}$$

The simple case of $q(\theta) = 1$ is used in the discussion later in this thesis. However, in general $q(\theta)$ can be any function of θ.

The uncoupled heat conduction equation has been reduced to a two dimensional case by setting the axial term (z-direction) equal to zero. Setting the axial term to zero is synonymous with saying the ends of the cylinder are insulated and the shape of the heat flux does not vary in the z-direction.

3.3 Development of Stationary Solution

We can assume a solution of the form:

$$\overline{T}(\bar{r}, \theta, \bar{t}) = \overline{R}(\bar{r})\overline{H}(\theta)\overline{\Phi}(\bar{t}) \tag{3.6}$$

Substituting (3.6) into the governing equation (3.2):

$$\overline{H\Phi R}'' + \frac{1}{\bar{r}}\overline{H\Phi R}' + \frac{1}{\bar{r}^2}\overline{H}''\overline{\Phi R} = \overline{HR\Phi}' \tag{3.7}$$

where the primes indicate derivatives.

Rearranging (3.7):

$$\frac{\overline{\Phi}'}{\overline{\Phi}} = \frac{1}{\overline{RH}}\left[\overline{R}''\overline{H} + \frac{1}{\bar{r}}\overline{R}'\overline{H} + \frac{1}{\bar{r}^2}\overline{RH}''\right] = -\alpha^2 \tag{3.8}$$

where α must be a constant, since $\overline{\Phi}'/\overline{\Phi}$ depends only on time and the middle term depends on space variables. Therefore the solution for $\overline{\Phi}(\bar{t})$ has the form:

$$\overline{\Phi}(\bar{t}) = C_0 \exp\left(-\alpha^2 \bar{t}\right) \tag{3.9}$$

Rearranging (3.8), we can write:

$$\frac{\overline{H}''}{\overline{H}} = -\bar{r}^2\alpha - \bar{r}^2 \frac{\overline{R}''}{\overline{R}} - \bar{r}\frac{\overline{R}'}{\overline{R}} = -\chi^2 \tag{3.10}$$

where χ must be a constant since $\overline{H}''/\overline{H}$ is a function of θ only and the middle term is a function of $\bar{r}$ only. Therefore, the solution for $\overline{H}(\theta)$ has the form:

$$\overline{H}(\theta) = C_1 \cos\chi\theta + C_2 \sin\chi\theta \tag{3.11}$$

where the required 2π periodicity implies $\chi_n = n$ ($n = 0,1,2,...$)

Substituting n for χ in (3.10) and rearranging, we get:

$$\bar{r}^2\overline{R}'' + \bar{r}\overline{R}' + \left(\alpha_n^2\bar{r}^2 - n^2\right)\overline{R} = 0 \tag{3.12}$$

which is Bessel's equation, which has a solution of the form:

$$\overline{R}_{nm}(\bar{r}) = C_3 J_n(\alpha_{nm}\bar{r}) + C_4 Y_n(\alpha_{nm}\bar{r}) \tag{3.13}$$

Equation (3.13) must satisfy the boundary conditions (3.3) and (3.4). Since the derivative of Bessel's function can be expressed as:

$$\frac{\partial\left(J_n(\alpha_{nm}\bar{r})\right)}{\partial\bar{r}} = \left[\frac{n}{\alpha_{nm}\bar{r}} J_n(\alpha_{nm}\bar{r}) - J_{n+1}(\alpha_{nm}\bar{r})\right]\alpha_{nm}, \text{ or}$$

$$\frac{\partial\left(J_n(\alpha_{nm}\bar{r})\right)}{\partial\bar{r}} = \left[J_{n-1}(\alpha_{nm}\bar{r}) - \frac{n}{\alpha_{nm}\bar{r}} J_n(\alpha_{nm}\bar{r})\right]\alpha_{nm}$$

the combination of the boundary conditions and $\overline{R}(\bar{r})$ can be expressed as:

$$C_3\left[\left(n+\bar{h}_{\text{out}}\right)J_n(\alpha_{nm}) - \alpha_{nm}J_{n+1}(\alpha_{nm})\right] + C_4\left[\left(n+\bar{h}_{\text{out}}\right)Y_n(\alpha_{nm}) - \alpha_{nm}Y_{n+1}(\alpha_{nm})\right] = 0 \tag{3.14}$$

$$C_3\left[\left(\frac{n}{\bar{r}_{\text{in}}} - \bar{h}_{\text{in}}\right)J_n(\alpha_{nm}\bar{r}_{\text{in}}) - \alpha_{nm}J_{n+1}(\alpha_{nm}\bar{r}_{\text{in}})\right] + C_4\left[\left(\frac{n}{\bar{r}_{\text{in}}} - \bar{h}_{\text{in}}\right)Y_n(\alpha_{nm}\bar{r}_{\text{in}}) - \alpha_{nm}Y_{n+1}(\alpha_{nm}\bar{r}_{\text{in}})\right] = 0$$

The above equation yields the following two expressions:

$$C_4 = -C_3 \frac{\left(n - \bar{r}_{in}\bar{h}_{in}\right) J_n\left(\alpha_{nm}\bar{r}_{in}\right) - \alpha_{nm}\bar{r}_{in} J_{n+1}\left(\alpha_{nm}\bar{r}_{in}\right)}{\left(n - \bar{r}_{in}\bar{h}_{in}\right) Y_n\left(\alpha_{nm}\bar{r}_{in}\right) - \alpha_{nm}\bar{r}_{in} Y_{n+1}\left(\alpha_{nm}\bar{r}_{in}\right)} \tag{3.15}$$

and α_{nm} must be a positive root of: (3.16)

$$\left.\begin{aligned}&\left[\left(n + \bar{h}_{out}\right) J_n\left(\alpha_{nm}\right) - \alpha_{nm} J_{n+1}\left(\alpha_{nm}\right)\right]\left[\left(\frac{n}{\bar{r}_{in}} - \bar{h}_{in}\right) Y_n\left(\alpha_{nm}\bar{r}_{in}\right) - \alpha_{nm} Y_{n+1}\left(\alpha_{nm}\bar{r}_{in}\right)\right] \\ &+\left[\left(\frac{n}{\bar{r}_{in}} - \bar{h}_{in}\right) J_n\left(\alpha_{nm}\bar{r}_{in}\right) - \alpha_{nm} J_{n+1}\left(\alpha_{nm}\bar{r}_{in}\right)\right]\left[\left(n + \bar{h}_{out}\right) Y_n\left(\alpha_{nm}\right) - \alpha_{nm} Y_{n+1}\left(\alpha_{nm}\right)\right]\end{aligned}\right\} = 0$$

Now if we substitute (3.9), (3.11), (3.13), and (3.15) into (3.6) and sum over the infinite series of eigenvalues:

$$\bar{T}\left(\bar{r}, \theta, \bar{t}\right) = \sum_{n=0}^{\infty}\sum_{m=0}^{\infty}\left(A_n \cos n\theta + B_n \sin n\theta\right) D_{nm} R_{nm}\left(\bar{r}\right) \exp\left(-\alpha_{nm}{}^2 \bar{t}\right) \tag{3.17}$$

where

$$R_{nm}\left(\bar{r}\right) = \left(J_n\left(\alpha_{nm}\bar{r}\right) - \frac{\left(n - \bar{r}_{in}\bar{h}_{in}\right) J_n\left(\alpha_{nm}\bar{r}_{in}\right) - \alpha_{nm}\bar{r}_{in} J_{n+1}\left(\alpha_{nm}\bar{r}_{in}\right)}{\left(n - \bar{r}_{in}\bar{h}_{in}\right) Y_n\left(\alpha_{nm}\bar{r}_{in}\right) - \alpha_{nm}\bar{r}_{in} Y_{n+1}\left(\alpha_{nm}\bar{r}_{in}\right)} Y_n\left(\alpha_{nm}\bar{r}\right) \right) \tag{3.18}$$

Comparing (3.18) with [Takeuti, 1980, equation 6] one can see Takeuti's equation 6 should read: $-\left(2\alpha_{nk}/\pi b\right)\left[\alpha_{nk}\left\{J_n\left(\alpha_{nk} r\right)....\right.\right.$

Multiplying both sides of (3.17) by: $\begin{pmatrix}\cos p\theta \\ \sin p\theta\end{pmatrix} R_{pl}\left(\bar{r}\right)$ and rearranging, we can write:

$$\begin{aligned}&\begin{pmatrix}A_n \\ B_n\end{pmatrix} D_{nm} \int_0^{2\pi}\begin{pmatrix}\cos n\theta \cos p\theta \\ \sin n\theta \sin p\theta\end{pmatrix} d\theta \int_{\bar{r}_{in}}^{1} R_{nm}\left(\bar{r}\right) R_{pl}\left(\bar{r}\right)\, d\bar{r} \\ &= Q_0 \int_0^{2\pi} q\left(\theta\right)\begin{pmatrix}\cos p\theta \\ \sin p\theta\end{pmatrix} d\theta \int_{\bar{r}_{in}}^{1} R_{pl}\left(\bar{r}\right) \frac{\delta\left(\bar{r} - 1\right)}{\bar{r}}\, d\bar{r}\end{aligned} \tag{3.19}$$

By enforcing orthogonality among the eigenfunctions in (3.19), and rearranging we can write:

$$\begin{pmatrix} A_p \\ B_p \end{pmatrix} D_{pl} \int_0^{2\pi} \begin{pmatrix} \cos^2 p\theta \\ \sin^2 p\theta \end{pmatrix} d\theta \int_{\bar{r}_{in}}^{1} R_{pl}^2(\bar{r})\bar{r}\, d\bar{r} = Q_0 \int_0^{2\pi} q(\theta) \begin{pmatrix} \cos p\theta \\ \sin p\theta \end{pmatrix} d\theta \int_{\bar{r}_{in}}^{1} R_{pl}(\bar{r})\delta(\bar{r}-1)\, d\bar{r} \qquad (3.20)$$

The integration of the left hand side of the above equation can be performed by noting that:

$$\int_{\bar{r}_{in}}^{\bar{r}_{out}} \bar{r} R_{nm}(\bar{r}) R_{nl}(\bar{r})\, d\bar{r} = \begin{cases} 0 & (m \neq n) \\ \left[\frac{1}{2}\bar{r}^2 \left[\left(1 - \frac{n}{\alpha_{nm}^2 \bar{r}^2} \right) R_{nm}^2(\bar{r}) + \left(\frac{\partial R_{nm}(\bar{r})}{\partial \bar{r}} \right)^2 \right] \right]_{\bar{r}_{in}}^{\bar{r}_{out}} & (m = n) \end{cases}$$

where $R_{nm}(\bar{r}) = C_3 J_n(\alpha_{nm}\bar{r}) + C_4 Y_n(\alpha_{nm}\bar{r})$ (eq. (3.18)), provided:

(1) α_{nm} is a real zero of $C_7 \alpha_{nm} R_{n+1}(\alpha_{nm}\bar{r}_{out}) - C_8 R_n(\alpha_{nm}\bar{r}_{out}) = 0$ (eq. (3.16)), and

(2) there must exist numbers k_1 and k_2 (both not zero), so that for all n: $C_9 \alpha_{nm} R_{n+1}(\alpha_{nm}\bar{r}_{in}) - C_{10} R_n(\alpha_{nm}\bar{r}_{in}) = 0$ (eq. (3.17))

Performing the integration of (3.20), changing the subscripts back, and noting that:

$$\frac{\partial R_{nm}}{\partial \bar{r}} = \frac{1}{\alpha_{nm}} \frac{dR_{nm}(\bar{r})}{d\bar{r}} = \frac{\bar{h}_{in}}{\alpha_{nm}} R_{nm}(\bar{r}_{in}) = -\frac{\bar{h}_{out}}{\alpha_{nm}} R_{nm}(1) \quad \text{at the boundaries ((3.2) and (3.3)),}$$

we can write:

$$\begin{pmatrix} A_n \\ B_n \end{pmatrix} D_{nm} \frac{\pi}{2} \left[\left(1 - \frac{n^2}{\alpha_{nm}^2} + \frac{\bar{h}_{out}^2}{\alpha_{nm}^2} \right) R_{nm}^2(1) - \left(\rho_1 - \frac{n^2}{\alpha_{nm}^2} + \frac{\bar{h}_{in}^2 \bar{r}_{in}^2}{\alpha_{nm}^2} \right) R_{nm}^2(\bar{r}_{in}) \right] \qquad (3.21$$

$$= R_{nm}(1) Q_0 \int_0^{2\pi} q(\theta) \begin{pmatrix} \cos n\theta \\ \sin n\theta \end{pmatrix} d\theta$$

Solving for the constants $A_n D_{nm}$ and $B_n D_{nm}$ in (3.21), we get:

$$A_0 D_{0m} = \frac{R_{0m}(1) Q_0 \int_{-\beta}^{\beta} q(\theta')\, d\theta'}{\pi\left[\left(1+\frac{h_{out}^2}{\alpha_{0m}^2}\right) R_{0m}^2(1) - \left(\bar{r}_{in} + \frac{\bar{h}_{in}^2 \bar{r}_{in}^2}{\alpha_{0m}^2}\right) R_{0m}^2(\bar{r}_{in})\right]}$$

$$\begin{pmatrix} A_n \\ B_n \end{pmatrix} D_{nm} = \frac{2 R_{nm}(1) Q_0 \int_{-\beta}^{\beta} q(\theta') \begin{pmatrix} \cos n\theta' \\ \sin n\theta' \end{pmatrix} d\theta'}{\pi\left[\left(1-\frac{n^2}{\alpha_{nm}^2}+\frac{h_{out}^2}{\alpha_{nm}^2}\right) R_{nm}^2(1) - \left(\bar{r}_{in} - \frac{n^2}{\alpha_{nm}^2} + \frac{\bar{h}_{in}^2 \bar{r}_{in}^2}{\alpha_{nm}^2}\right) R_{nm}^2(\bar{r}_{in})\right]} \tag{3.22}$$

Equation (3.17) with constants (3.22) describe the stationary two dimensional response of an arbitrary distributed heat flux on the outer surface of a cylinder with convective boundary conditions on the inner and outer radius.

3.4 TRANSIENT SOLUTION

By replacing θ by $(\theta - \bar{\omega}\bar{t}')$ and $\bar{t}$ by $(\bar{t} - \bar{t}')$ where $\bar{\omega} = \omega_{cam} r_{out}^2 / \kappa$ (3.17) and integrating over time, the steady state solution can be made to represent the dynamic solution (3.23).

$$\bar{T}_\omega = \sum_{n=0}^{\infty}\sum_{m=1}^{\infty} \begin{aligned} &A_n D_{nm} R_{nm}(\bar{r}) \int_0^{\bar{t}} \cos n(\theta - \bar{\omega}\bar{t}') \exp\left(-\alpha_{nm}^2 (\bar{t} - \bar{t}')\right) d\bar{t}' \\ &+ B_n D_{nm} R_{nm}(\bar{r}) \int_0^{\bar{t}} \sin n(\theta - \bar{\omega}\bar{t}') \exp\left(-\alpha_{nm}^2 (\bar{t} - \bar{t}')\right) d\bar{t}' \end{aligned} \tag{3.23}$$

The subscript, ω, on $\bar{T}_\omega$ is used to indicate the dynamic solution. Recalling that:

$$\cos n(\theta - \bar{\omega}\bar{t}') = \cos(n\theta)\cos(n\bar{\omega}\bar{t}') + \sin(n\theta)\sin(n\bar{\omega}\bar{t}')$$

$$\sin n(\theta - \bar{\omega}\bar{t}') = \sin(n\theta)\cos(n\bar{\omega}\bar{t}') - \cos(n\theta)\sin(n\bar{\omega}\bar{t}')$$

$$\int \exp(\alpha_{nm}^2 \bar{t}')\cos(n\omega\bar{t}')\, d\bar{t}' = \frac{\exp(\alpha_{nm}^2 \bar{t}')\left[\alpha_{nm}^2 \cos(n\omega\bar{t}') + n\omega \sin(n\omega\bar{t}')\right]}{\alpha_{nm}^4 + n^2\omega^2}$$

$$\int \exp(\alpha_{nm}^2 \bar{t}')\sin(n\omega\bar{t}')\, d\bar{t}' = \frac{\exp(\alpha_{nm}^2 \bar{t}')\left[\alpha_{nm}^2 \sin(n\omega\bar{t}') - n\omega \cos(n\omega\bar{t}')\right]}{\alpha_{nm}^4 + n^2\omega^2}$$

the integration on (3.23), yields the solution of the original problem posed in Figure 3-3, with the governing equation (3.2) and boundary conditions (3.3)-(3.5)as stated.

$$\bar{T}_{\omega} = \sum_{n=0}^{\infty}\sum_{m=1}^{\infty} G_{nm}^{(1)}(\bar{r},\bar{t})\cos n\theta + \sum_{n=1}^{\infty}\sum_{m=1}^{\infty} G_{nm}^{(2)}(\bar{r},\bar{t})\sin n\theta \tag{3.24}$$

where:

$$G_{nm}^{(1)}(\bar{r},\bar{t}) = D_{nm}R_{nm}(\bar{r})\frac{\left\{\begin{array}{l} A_n\left[\alpha_{nm}^2\cos(n\bar{\omega}) + n\bar{\omega}\sin(n\bar{\omega}\bar{t}) - \alpha_{nm}^2\exp(-\alpha_{nm}^2\bar{t})\right] \\ \quad + B_n\left[n\bar{\omega}\cos(n\bar{\omega}\bar{t}) - \alpha_{nm}^2\sin(n\bar{\omega}\bar{t}) - n\bar{\omega}\exp(-\alpha_{nm}^2\bar{t})\right] \end{array}\right\}}{\alpha_{nm}^4 + n^2\bar{\omega}^2} \tag{3.25}$$

$$G_{nm}^{(2)}(\bar{r},\bar{t}) = D_{nm}R_{nm}(\bar{r})\frac{\left\{\begin{array}{l} A_n\left[\alpha_{nm}^2\sin(n\bar{\omega}\bar{t}) - n\bar{\omega}\cos(n\bar{\omega}\bar{t}) + n\bar{\omega}\exp(-\alpha_{nm}^2\bar{t})\right] \\ \quad + B_n\left[n\bar{\omega}\sin(n\bar{\omega}\bar{t}) + \alpha_{nm}^2\cos(n\bar{\omega}\bar{t}) - \alpha_{nm}^2\exp(-\alpha_{nm}^2\bar{t})\right] \end{array}\right\}}{\alpha_{nm}^4 + n^2\bar{\omega}^2}$$

and where:

$$A_0 = \frac{1}{2}\int_{-\beta}^{\beta} q(\theta')\, d\theta'$$

$$\begin{pmatrix} A_n \\ B_n \end{pmatrix} = \int_{-\beta}^{\beta} q(\theta')\begin{pmatrix} \cos n\theta' \\ \sin n\theta' \end{pmatrix} d\theta'$$

$$D_{nm} = \frac{2R_{nm}(1)Q_0}{\pi\left[\left(1 - \frac{n^2}{\alpha_{nm}^2} + \frac{h_{\text{out}}^2}{\alpha_{nm}^2}\right)R_{nm}^2(1) - \left(\bar{r}_{\text{in}} - \frac{n^2}{\alpha_{nm}^2} + \frac{\bar{h}_{\text{in}}^2\bar{r}_{\text{in}}^2}{\alpha_{nm}^2}\right)R_{nm}^2(\bar{r}_{\text{in}})\right]}$$

$$R_{nm}(\bar{r}) = \left(J_n(\alpha_{nm}\bar{r}) - \frac{(n - \bar{r}_{\text{in}}\bar{h}_{\text{in}})J_n(\alpha_{nm}\bar{r}_{\text{in}}) - \alpha_{nm}\bar{r}_{\text{in}}J_{n+1}(\alpha_{nm}\bar{r}_{\text{in}})}{(n - \bar{r}_{\text{in}}\bar{h}_{\text{in}})Y_n(\alpha_{nm}\bar{r}_{\text{in}}) - \alpha_{nm}\bar{r}_{\text{in}}Y_{n+1}(\alpha_{nm}\bar{r}_{\text{in}})}Y_n(\alpha_{nm}\bar{r})\right)$$

The solution (3.24) is the two-dimensional version as presented in Takeuti, 1986, with the term $G_{nm}^{(1)}(\bar{t})$ corrected. Note that the term $D_{nm}R_{nm}(\bar{r})$ was not included as part of $G_{nm}^{(1)}(\bar{t})$ or $G_{nm}^{(2)}(\bar{t})$ in the analysis by Takeuti, but it facilitates the thermal stress analysis in Section 4.2. A graphical representation of (3.24) can be seen in Figure 3-4. Although

the $n = 0$ term is not written out exclusively, the $n = 0$ substitution into the solution stated will yield the correct answer.

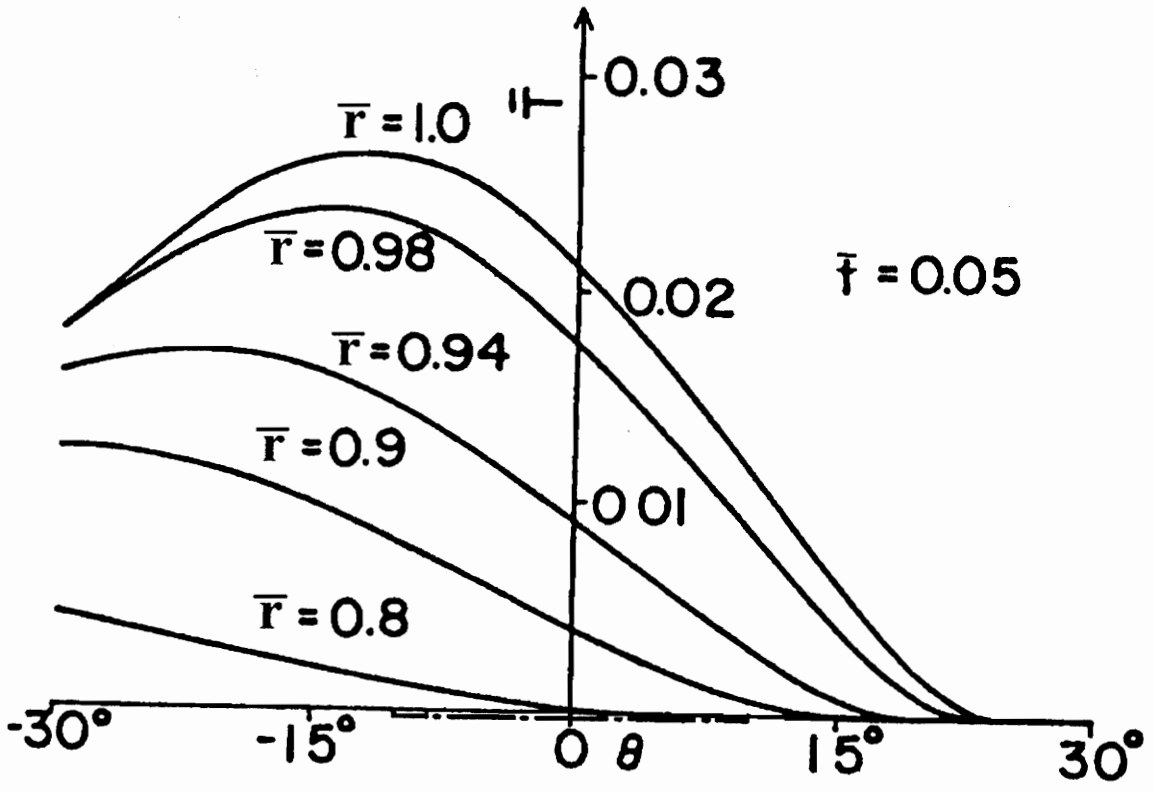

Figure 3-4 Graphical representation of solution to the problem posed in (3.2) and Figure 3-3 with the necessary parameters given below. The dashed line that represents the heat source and has been corrected from the original reference [Takeuti, 1986, p. 510].

parameters used to create the above graph:

$h_{in} = 0.1$	$h_{out} = 1.0$	$\overline{\omega} = 70$	$\beta = \frac{\pi}{36}$
$\bar{r}_{in} = 0.5$	$\nu = 0.3$	$q(\theta) = 1$	$\bar{t} = 0.05$

3.5 ENERGY PARTITION IN GRINDING ZONE*

Essentially all of the power expended during a grinding process is dissipated in the form of heat in the grinding zone [Outwater, 1952]. Portions of the total heat generated are absorbed by the grinding fluid, conducted into the abrasive grains and subsequently convected away by the motion of the grinding wheel, removed by the grinding swarf, and conducted into the workpiece (see Figure 3-5 and Figure 3-6). The fractions of the grinding energy leaving the grinding zone by these different methods is known as the energy partition.

The solution developed in Section 3.4 would be more robust if an energy partition was used to calculate the portion of heat conducted into the workpiece. This quantity can be substituted for $Q_0 q(\theta)$ in Figure 3-3.

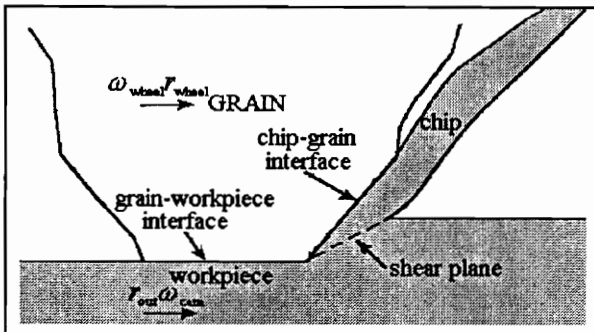

Figure 3-5 Locations of heat generation [Lavine, 1991, p. 985]

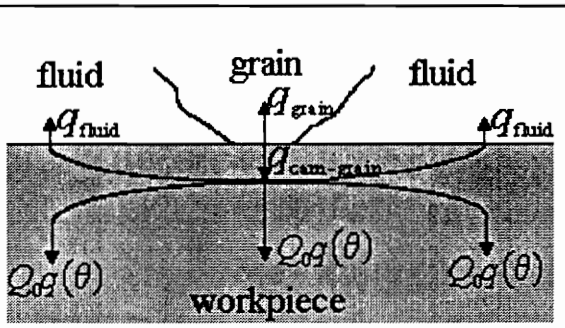

Figure 3-6 Heat transfer paths [Lavine, 1991, p. 985]

An extensive model has been developed to determine the energy partition in the grinding zone [Lavine, 1991]. The model considers the heat transfer in the grinding zone. It accounts for heat removed by conduction into the wheel, convection into the

* Modified version of that developed by [Lavine, 1991]

grinding fluid and conduction into the workpiece (see Figure 3-6). The model predicts the occurrence of film boiling and thermal damage to the workpiece.

Lavine's model starts with the uncoupled heat conduction equation (2.26) and the assumptions inherent in using it. It does not account for radiation or heat removed by the grinding swarf. Each grain is assumed to be the frustum of a cone. Heat that conducts into the grain is assumed to remain in the grain and not be removed by the grinding fluid. The heat flux from the grain into the workpiece is assumed to be a constant band source, infinite in length in the direction of the wheel rotational rate vector (ω_{wheel}, Figure 3-5), at the point of contact. The infeed rate of the material is assumed to be fast enough to neglect conduction in the direction of motion (ω_{wheel}, Figure 3-5). The entire model is developed, then coupled by enforcing the fact that the temperature at the interface must agree for each solution. The portion of Lavine's solution which is useful here is written below for reference. Note that the author has adapted Lavine's nomenclature to suit the case of interest.

$$Q_0 q(\theta) = \frac{F_{\tan}\omega_{\text{wheel}}}{\left[1+\frac{h_{\text{fluid}}}{h_{\text{cam}}}(1-A)\right]\left[1+\frac{\bar{h}_{\text{grain}}}{\bar{h}_{\text{cam-grain}}}\right]+A\overline{\left(h_{\text{grain}}/h_{\text{cam-grain}}\right)}} \tag{3.26}$$

$$h_{\text{fluid}}\left(r_{\text{out}}(\theta-\beta)\right) = \sqrt{\pi\left(k\rho\tilde{c}\right)_{\text{fluid}}\omega_{\text{wheel}}r_{\text{wheel}}/4\left[r_{\text{out}}(\theta-\beta)\right]}$$

$$h_{\text{cam}}\left(r_{\text{out}}(\theta-\beta)\right) = \sqrt{\pi\left(k\rho\tilde{c}\right)_{\text{cam}}\omega_{\text{cam}}r_{\text{out}}/4\left[r_{\text{out}}(\theta-\beta)\right]}$$

$$\frac{\bar{h}_{\text{grain}}}{\bar{h}_{\text{cam-grain}}} = \sqrt{\frac{\left(k\rho\tilde{c}\right)_{\text{grain}}}{\left(k\rho\tilde{c}\right)_{\text{cam}}}}I_2\left(L_{\text{grain}}\right)\frac{1}{4L\sqrt{\pi}}\int_0^L f\left(L,L_{\text{grain}},\kappa_{\text{grain}}/\kappa_{\text{cam}}\right)\sqrt{X}\,dX$$

$$\overline{\left(h_{\text{grain}}/h_{\text{cam-grain}}\right)} = \sqrt{\frac{\left(k\rho\tilde{c}\right)_{\text{grain}}\omega_{\text{wheel}}r_{\text{wheel}}}{\left(k\rho\tilde{c}\right)_{\text{cam}}\omega_{\text{cam}}r_{\text{out}}}}\frac{1}{L}\int_0^L f\left(L,L_{\text{grain}},\kappa_{\text{grain}}/\kappa_{\text{cam}}\right)dX$$

$$I_2\left(L_{\text{grain}}\right) = \frac{1}{L_{\text{grain}}^2}\int_0^{L_{\text{grain}}}\int_0^{L_{\text{grain}}}\left\{\int_Y^{Y-L_{\text{grain}}}\int_X^{X-L_{\text{grain}}}\frac{\exp\left(-\sqrt{\xi^2+\eta^2}-\xi\right)}{\sqrt{\xi^2+\eta^2}}d\xi d\eta\right\}dX\,dY$$

$$f\left(L, L_{\text{grain}}, \kappa_{\text{grain}}/\kappa_{\text{cam}}\right) = \frac{2\sqrt{\pi X \kappa_{\text{grain}}/L_{\text{grain}}^2 \kappa_{\text{cam}}}}{\sqrt{\pi}\left\{1-\exp\left(\pi X \kappa_{\text{grain}}/L_{\text{grain}}^2 \kappa_{\text{cam}}\right) erfc\left(\sqrt{\pi X \kappa_{\text{grain}}/L_{\text{grain}}^2 \kappa_{\text{cam}}}\right)\right\}}$$

$$A = A_{\text{grain}}/(2\beta r_{\text{out}} l_{\text{cam}}); \quad L = 2\omega_{\text{wheel}} r_{\text{wheel}} \beta r_{\text{out}}/\kappa_{\text{cam}}; \quad L_{\text{grain}} = \omega_{\text{wheel}} r_{\text{wheel}} l_{\text{grain}}/\kappa_{\text{cam}}$$

where l_{grain} is the width of the aforementioned band source of heat.

Lavine found her theoretical predictions were in excellent agreement with experimental data. The most influential parameters proved to be the grinding fluid type and the grain type used in the grinding wheel. Grinding zone length and grain-workpiece contact area were second order effects. The model also incorporated film boiling using empirical data found in previous studies [Ohishi, 1985],[Yasui, 1983] by setting $h_{\text{fluid}} = 0$ when the calculated temperatures reach the experimental values for film boiling.

4. ANALYTIC STRESS PROFILES DURING GRINDING

"c e i i i n o s s s t t u v" -Robert Hooke[*], Book of the Description of Helioscopes. *The solution to this Latin anagram is "Ut tensio sic vis." Translation: The power of any spring is in the same proportion with the tension thereof. This anagram is the renowned Hooke's Law.*

Mechanical pressures of the grinding wheel, thermal gradients, and phase transformations develop the stresses experienced by the workpiece during grinding. Stresses due to phase transformations will not be considered in this analysis. Assumptions inherent in the equations of linear thermoelasticity (2.34) and elasticity (2.31) as developed in Section 2.1.5 and 2.1.6 are assumed valid.

4.1 RESTRICTIONS OF A TWO DIMENSIONAL ANALYSIS

Continuing the two dimensional restriction placed on the heat conduction equation(3.2), an analogous restriction should be placed on the equations of elasticity (2.31) and thermoelasticity (2.34). A two dimensional analysis can be performed by making an assumption that either the stress (plane stress - see Figure 4-1), or the strain in one direction is zero (plane strain - see Figure 4-2).

[*] Robert Hooke (1635 - 1703): English philosopher, microscopist, and physicist.

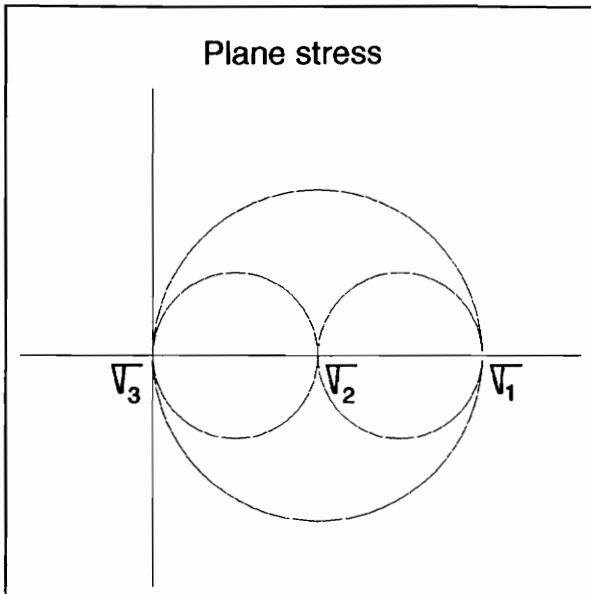

Figure 4-1 Mohr's circle representing plane stress ($\sigma_{zz} = 0$)

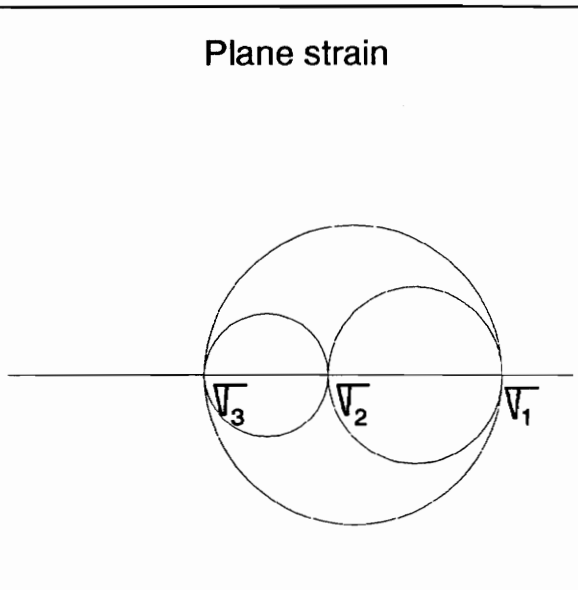

Figure 4-2 Mohr's circle representing plane strain ($\sigma_{zz} = \nu[\sigma_{rr} + \sigma_{\theta\theta}] + \alpha_{th}ET$)

The problem of a solid cylinder of radius r_{out} and length b can be reduced to either plane stress or plane strain. If the ratio r_{out}/b is small compared to unity and the ends are free of traction, the stress state of the cylinder can be represented as plane stress (see Figure 4-1). Conversely, if the ratio r_{out}/b is large compared to unity so displacements can be considered constrained in the axial direction, the cylinder can be considered to be in a state of plane strain (see Figure 4-2) [Boley, 1985, p. 288].

Using the present local radius of curvature/cylinder assumption and considering the cams are 15.8 millimeters in length, the cam can be seen to be in neither plane-strain nor plane-stress (see Figure 3-1) for cylinder radii. Therefore, the cam is assumed to be in plane stress near the edges and assumed to be in plane strain near the center

4.2 STRESSES DUE TO THERMAL GRADIENTS*

Although the thermoelasticity solution to the temperature distribution (3.24) is known [Takeuti, 1986], the derivation was not published. A method of solution is published here for completeness and understanding.

For a circular disc or cylinder with a plane-harmonic temperature distribution such as the one developed in Section 3.2, a solution can be found in terms of the well-known Airy's stress function φ, which in turn yields stresses.

Governing Equation: $\nabla^4\overline{\varphi} + \bar{r}_{\text{in}}^2(1-\upsilon)\nabla^2\overline{T} = 0$ **(4.1)**

Boundary Conditions: **(4.2)**

$$\overline{\varphi} = \frac{\partial\overline{\varphi}}{\partial\bar{r}} = 0; \qquad \bar{r} = 1$$

$$\left.\begin{aligned} \overline{\varphi} &= C_{12}\bar{r}\cos(\theta) + C_{13}\bar{r}\sin(\theta) + C_{14} \\ \frac{\partial\overline{\varphi}}{\partial\bar{r}} &= C_{12}\cos(\theta) + C_{13}\sin(\theta) \end{aligned}\right\} \qquad \bar{r} = \bar{r}_{\text{in}} \tag{4.3}$$

where C_{12}, C_{13} and C_{14} are arbitrary constants.

Michell Conditions: **(4.4)**

$$\left.\begin{aligned} \int_0^{2\pi}\left(\frac{\partial\nabla^2\overline{\varphi}}{\partial\bar{r}}\bar{r}\sin\theta - \frac{\partial\nabla^2\overline{\varphi}}{\rho\partial\theta}\bar{r}\cos\theta\right)\bar{r}\,d\theta &= -\bar{r}_{in}^2(1-\nu)\int_0^{2\pi}\left(\frac{\partial\overline{T}}{\partial\bar{r}}\bar{r}\sin\theta - \frac{\partial\overline{T}}{\bar{r}\partial\theta}\bar{r}\cos\theta\right)\bar{r}\,d\theta \\ \int_0^{2\pi}\left(\frac{\partial\nabla^2\overline{\varphi}}{\partial\bar{r}}\bar{r}\cos\theta + \frac{\partial\nabla^2\overline{\varphi}}{\rho\partial\theta}\bar{r}\sin\theta\right)\bar{r}\,d\theta &= -\bar{r}_{in}^2(1-\nu)\int_0^{2\pi}\left(\frac{\partial\overline{T}}{\partial\bar{r}}\bar{r}\cos\theta + \frac{\partial\overline{T}}{\bar{r}\partial\theta}\bar{r}\sin\theta\right)\bar{r}\,d\theta \end{aligned}\right\} \bar{r} = \bar{r}_{\text{in}}$$

$$\int_0^{2\pi}\frac{\partial\nabla^2\overline{\varphi}}{\partial\bar{r}}\bar{r}\,d\theta = -\bar{r}_{\text{in}}^2(1-\nu)\int_0^{2\pi}\frac{\partial\overline{T}}{\partial\bar{r}}\bar{r}\,d\theta; \qquad \bar{r} = \bar{r}_{\text{in}} \tag{4.5}$$

The boundary (4.2) and Michell (4.5) conditions arise from the compatibility equations (2.3) when they are expressed in terms of the Airy's stress function [see Boley, 1985, equation 3.6.20 and pp. 112 - 115]. The solution to equation (4.1) is of the form:

---

* See [Boley, 1985, pp. 292-298] for an explanation of terms and a more in-depth treatment

$$\bar{\varphi}(\bar{r},\theta,\bar{t}) = \sum_{n=0}^{\infty} g_n^{(1)}(\bar{r},\bar{t})\cos(n\theta) + \sum_{n=1}^{\infty} g_n^{(2)}(\bar{r},\bar{t})\sin(n\theta) \tag{4.6}$$

Substituting the heat conduction equation (3.24), corresponding boundary conditions (3.3) to (3.5), and equation (4.6) into equations (4.1) - (4.5), the solution for $g_n^{(1)}$ and $g_n^{(2)}$ is the solution to:

$$\frac{\partial^4 g_n}{\partial \bar{r}^4} + \frac{2}{\bar{r}}\frac{\partial^3 g_n}{\partial \bar{r}^3} - \frac{1+2n^2}{\bar{r}^2}\frac{\partial^2 g_n}{\partial \bar{r}^2} + \frac{1+2n^2}{\bar{r}^3}\frac{\partial g_n}{\partial \bar{r}} + \frac{n^2\left(n^2-4\right)}{\bar{r}^4} g_n = 0 \tag{4.7}$$

Boundary Conditions: **(4.8)**

$$g_n(1) = \frac{\partial g_n(1)}{\partial \bar{r}} = 0$$

$$g_0^{(1)}(\bar{r}_{\text{in}}) = C_{14}; \quad g_n^{(1)}(\bar{r}_{\text{in}}) = C_{12}\bar{r}_{\text{in}}\cos n\theta; \quad \frac{\partial g_0^{(1)}(\bar{r}_{\text{in}})}{\partial \bar{r}} = 0; \quad \frac{\partial g_n^{(1)}(\bar{r}_{\text{in}})}{\partial \bar{r}} = C_{12}\cos n\theta \tag{4.9}$$

$$g_n^{(2)}(\bar{r}_{\text{in}}) = C_{13}\bar{r}_{\text{in}}\sin n\theta; \quad \frac{\partial g_n^{(2)}(\bar{r}_{\text{in}})}{\partial \bar{r}} = C_{13}\sin n\theta \tag{4.10}$$

Michell Conditions **(4.11)**

$$\frac{d}{d\bar{r}}\left[\frac{1}{\bar{r}}\frac{d}{d\bar{r}}\left(\bar{r}\frac{dg_0^{(1)}(\bar{r}_{\text{in}})}{d\bar{r}}\right)\right] = -\bar{r}_{in}^2(1-\nu)\frac{dG_0^{(1)}(\bar{r}_{\text{in}})}{d\bar{r}}$$

$$\left(\frac{1}{\bar{r}} - \frac{d}{d\bar{r}}\right)\frac{d}{d\bar{r}}\left[-\frac{g_n(\bar{r}_{\text{in}})}{\bar{r}^2} + \frac{1}{\bar{r}}\frac{d}{d\bar{r}}\left(\bar{r}\frac{dg_n(\bar{r}_{\text{in}})}{d\bar{r}}\right)\right] = -\bar{r}_{\text{in}}^2(1-\nu)\left(\frac{1}{\bar{r}} - \frac{d}{d\bar{r}}\right)G_n(\bar{r}_{\text{in}}) \tag{4.12}$$

where $g_n = g_n^{(1)}, g_n^{(2)}$ (4.6) and $G_n = \sum_{m=1}^{\infty} G_{nm}^{(1)}, \sum_{m=1}^{\infty} G_{nm}^{(2)}$ (3.25) unless noted otherwise.

The solutions to the two separate problems posed in equations (4.7) to (4.12) is:

$$g_0^{(1)}(\bar{r},\bar{t}) = \left\{ \begin{array}{l} K_0^{(1)} + L_0^{(1)} \ln \bar{r} + M_0^{(1)} \bar{r}^2 + N_0^{(1)} \bar{r}^2 \ln \bar{r} \\ \quad + \bar{r}_{\text{in}}^2 (1-\nu) \left[\bar{r} \int_{\bar{r}_{\text{in}}}^{\bar{r}} G_0^{(1)}(\bar{r}',\bar{t}) \bar{r}' \ln \bar{r}' d\bar{r}' - \ln \bar{r} \int_{\bar{r}_{\text{in}}}^{\bar{r}} G_0^{(1)}(\bar{r}',\bar{t}) \bar{r}' d\bar{r}' \right] \end{array} \right\} \tag{4.13}$$

$$g_1^{(1)}(\bar{r},\bar{t}) = \left\{ \begin{array}{l} K_1^{(1)} \bar{r} + \dfrac{L_1^{(1)}}{\bar{r}} + M_1^{(1)} \bar{r}^3 + N_1^{(1)} \bar{r} \ln \bar{r} \\ \quad + \dfrac{\bar{r}_{\text{in}}^2 (1-\nu)}{2} \left[\begin{array}{l} \bar{r} \displaystyle\int_{\bar{r}_{\text{in}}}^{\bar{r}} G_1^{(1)}(\bar{r}',\bar{t}) (\bar{r}')^2 \, d\bar{r}' \\ -\bar{r} \displaystyle\int_{\bar{r}_{\text{in}}}^{\bar{r}} G_1^{(1)}(\bar{r}',\bar{t}) \, d\bar{r}' \end{array} \right] \end{array} \right\} \cos\theta$$

$$g_n^{(1)}(\bar{r},\bar{t}) = \left\{ \begin{array}{l} K_n^{(1)} \bar{r}^{-n} + L_n^{(1)} \bar{r}^n + M_n^{(1)} \bar{r}^{-n+2} + N_n^{(1)} \bar{r}^{n-2} \\ \quad + \dfrac{\bar{r}_{\text{in}}^2 (1-\nu)}{2n} \left[\begin{array}{l} \bar{r}^{-n} \displaystyle\int_{\bar{r}_{\text{in}}}^{\bar{r}} G_n^{(1)}(\bar{r}',\bar{t}) (\bar{r}')^{n+1} \, d\bar{r}' \\ -\bar{r}^n \displaystyle\int_{\bar{r}_{\text{in}}}^{\bar{r}} G_n^{(1)}(\bar{r}',\bar{t}) (\bar{r}')^{-n+1} \, d\bar{r}' \end{array} \right] \end{array} \right\} \cos n\theta \tag{4.14}$$

$$g_1^{(2)}(\bar{r},\bar{t}) = \left\{ \begin{array}{l} K_1^{(2)} \bar{r} + \dfrac{K_1^{(2)}}{\bar{r}} + K_1^{(2)} \bar{r}^3 + K_1^{(2)} \bar{r} \ln \bar{r} \\ \quad + \dfrac{\bar{r}_{\text{in}}^2 (1-\nu)}{2} \left[\begin{array}{l} \bar{r}^{-1} \displaystyle\int_{\bar{r}_{\text{in}}}^{\bar{r}} G_1^{(2)}(\bar{r}',\bar{t}) (\bar{r}')^2 \, d\bar{r}' \\ -\bar{r} \displaystyle\int_{\bar{r}_{\text{in}}}^{\bar{r}} G_1^{(2)}(\bar{r}',\bar{t}) \, d\bar{r}' \end{array} \right] \end{array} \right\} \sin\theta \tag{4.15}$$

$$g_n^{(2)}(\bar{r},\bar{t}) = \left\{ \begin{array}{l} K_n^{(2)} \bar{r}^{-n} + L_n^{(2)} \bar{r}^n + M_n^{(2)} \bar{r}^{-n+2} + N_n^{(2)} \bar{r}^{n-2} \\ \quad + \dfrac{\bar{r}_{\text{in}}^2 (1-\nu)}{2n} \left[\begin{array}{l} \bar{r}^{-n} \displaystyle\int_{\bar{r}_{\text{in}}}^{\bar{r}} G_n^{(2)}(\bar{r}',\bar{t}) (\bar{r}')^{n+1} \, d\bar{r}' \\ -\bar{r}^n \displaystyle\int_{\bar{r}_{\text{in}}}^{\bar{r}} G_n^{(2)}(\bar{r}',\bar{t}) (\bar{r}')^{-n+1} \, d\bar{r}' \end{array} \right] \end{array} \right\} \sin n\theta \quad n = 2,3,4,... \tag{4.16}$$

The solution to Airy's stress function is found by substituting (4.13) through (4.16) into (4.6). The constants K_n, L_n, M_n, and N_n (n = 0, 1, 2, ...) are found by

considering the boundary conditions for stress, their relationship with Airy's stress function and satisfying them for each n.

$$\bar{\sigma}_{\bar{r}\bar{r}} = \frac{1}{\bar{r}}\frac{\partial\bar{\varphi}}{\partial\bar{r}} + \frac{1}{\bar{r}^2}\frac{\partial^2\bar{\varphi}}{\partial\theta^2} \tag{4.17}$$

$$\bar{\sigma}_{\theta\theta} = \frac{\partial^2\bar{\varphi}}{\partial\bar{r}^2} \tag{4.18}$$

$$\bar{\sigma}_{\bar{r}\theta} = -\frac{\partial}{\partial\bar{r}}\left(\frac{1}{\bar{r}}\frac{\partial\bar{\varphi}}{\partial\theta}\right) \tag{4.19}$$

$$\bar{\sigma}_{\bar{z}\bar{z}} = \begin{cases} 0 & plane-stress \\ \nu(\bar{\sigma}_{\bar{r}\bar{r}} + \bar{\sigma}_{\theta\theta}) + \bar{r}_{in}^2(1-\nu)\bar{T} & plane-strain \end{cases} \tag{4.20}$$

Boundary conditions:

$$\begin{aligned} \bar{\sigma}_{\bar{r}\bar{r}}(1,\theta,\bar{t}) &= \bar{\sigma}_{\bar{r}\bar{r}}(\bar{r}_{in},\theta,\bar{t}) = 0 \\ \bar{\sigma}_{\bar{r}\theta}(1,\theta,\bar{t}) &= \bar{\sigma}_{\bar{r}\theta}(\bar{r}_{in},\theta,\bar{t}) = 0 \end{aligned} \tag{4.21}$$

where the bar denotes non-dimensional stress. (4.22)

$$\bar{\sigma} = \frac{k}{r_{out}Q_0}\frac{\bar{r}_{in}^2(1-\nu)}{\alpha_{th}E}\sigma$$

The results of such an analysis for the specific case of Figure 3-3 are displayed in Figure 4-3. These equations were developed based on [Boley, 1985] and provide forms forms that could be used for numerical calculations. However, the calculations themselves were attempted but not completed for this thesis due to the extensive and complex programming required.

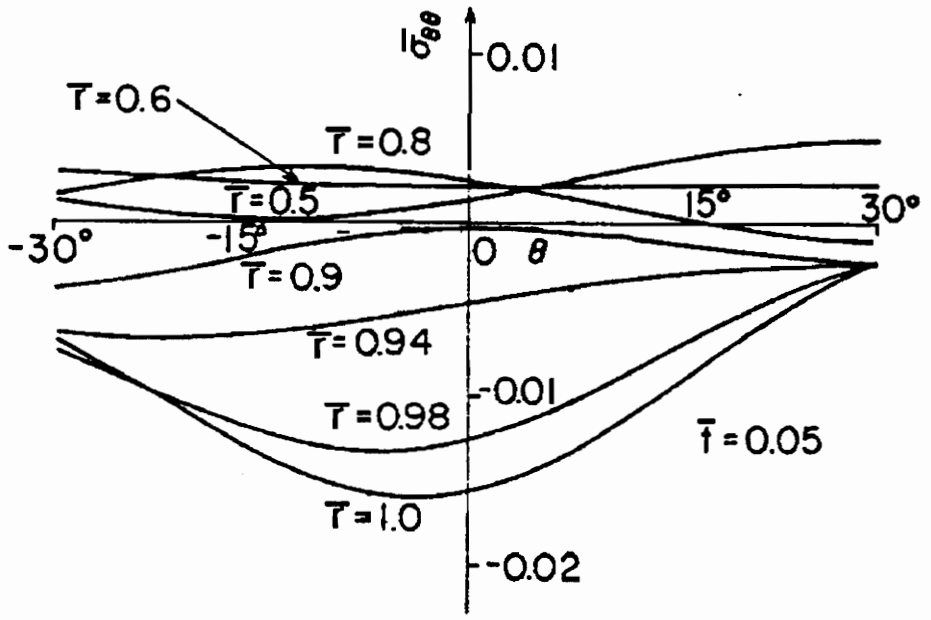

Figure 4-3 Non-dimensional hoop stress distribution due to thermal gradients at various non-dimensional depths [adapted from Takeuti, 1986]

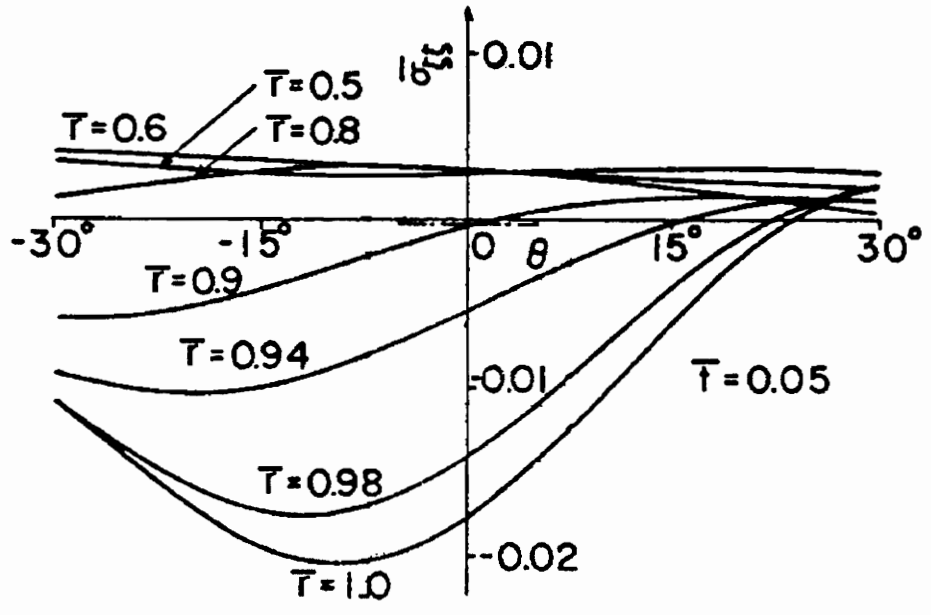

Figure 4-4 Non-dimensional axial stress due to thermal gradients at various non-dimensional depths for the plane-strain assumption [adapted from Takeuti, 1986]

For the plane-strain assumption, an axial stress is present (see Figure 4-2 and Figure 4-4). The plots depicted in Figure 4-3 and Figure 4-4 were created using the same parameters as Figure 3-4.

The hoop stress is the only stress investigated here since it is the greatest stress component (in plane-stress) and approximate plasticity corrections are being implemented to achieve the goal of predicting residual stress. However, if it is desired to view all stress components developed during grinding, it is certainly possible.

4.3 STRESSES DUE TO MECHANICAL WORKING

It has been shown that residual stresses due to grinding can be predicted at depths in excess of 20 microns within reasonable accuracy by considering only the thermal stresses induced by grinding. [Vansevenant, 1987, pp. 6-1 - 6-12] It has also been shown that fatigue-based failure (i.e. pitting or spalling) in roller-follower type camshafts initiates subsurface at depths of 25 to 150 microns [Girardin, 1994]. Therefore, the effects of mechanical pressures during grinding were investigated. Again, this is an elastic analysis and material properties are assumed constant with respect to temperature. The two cases of plane-strain and plane stress are investigated.

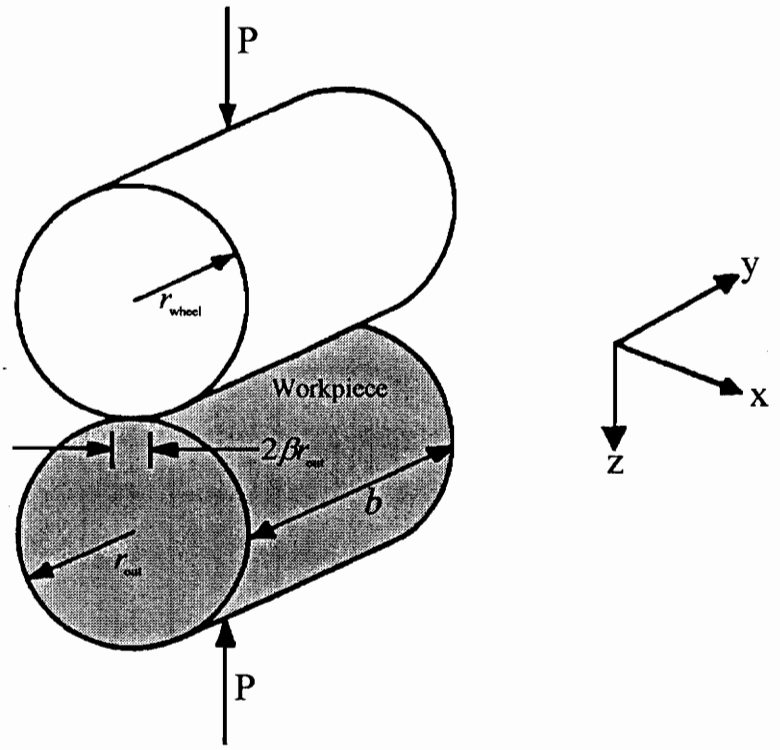

Figure 4-5 Contacting parallel cylinders with normal and tangential loading

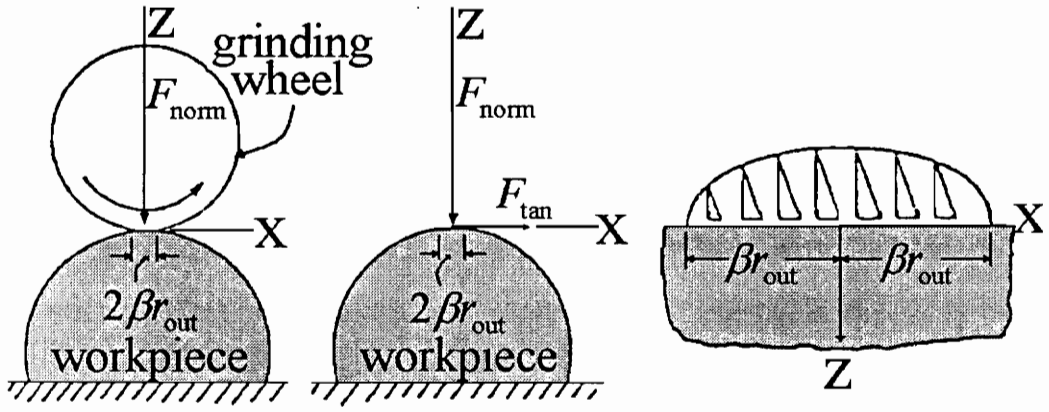

Figure 4-6 Normal and tangential pressure distributions [Adapted from Smith, 1953]

The case of two parallel cylinders in contact as developed by Smith and Lui is used for this analysis. One cylinder represents the grinding wheel, the other the local

radius of curvature. Each cylinder is given characteristic material properties and radii, either that of the cam or the wheel. The problem is separated into two elasticity problems; one for the normal load and one for the tangential load. Then the two solutions are superimposed using the principle of superposition.

4.3.1 NORMAL LOAD

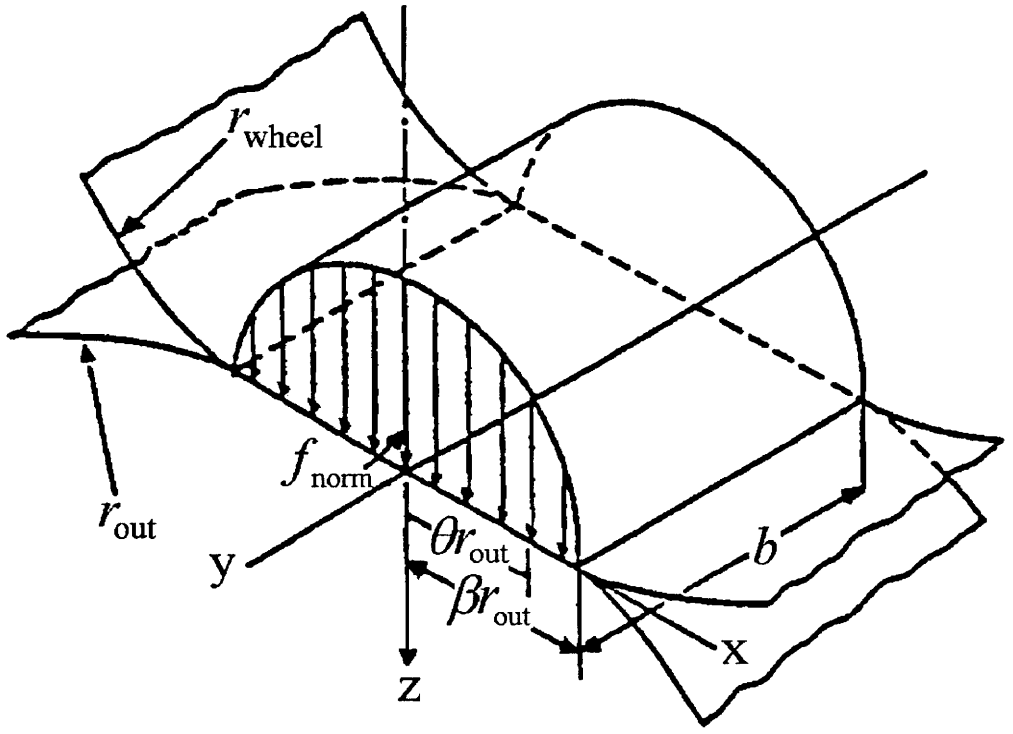

Figure 4-7 Normal pressure distribution in detail [Adapted from Juvinall, 1967]

4.3.1.1 CONTACT LENGTH

The normal load dictates the contact length, and therefore the contact area. Researchers have investigated the contact length in grinding extensively. Because wheel and workpiece deformation influence the geometric contact length, the real contact length is quite hard to predict. A number of analytic models have been developed using Hertzian theory [Hahn, 1967],[Lindsay, 1971a],[Lindsay, 1971b],[Hahn, 1976],[Verkerk, 1975],[Brown, 1971],[Sauer, 1974]. However, even the most accurate model [Verkerk, 1975] underestimates the real contact length by 100% at high speeds of grinding. Therefore, empirical models have been developed to more accurately predict the contact length. [Aerens, 1983],[Brandin, 1978] Vansevenant, 1987 has a concise summary of these models.

Classic Hertzian theory predicts half contact length to be defined by equation (4.23), which is the contact length used in this analysis.

$$\beta r_{out} = \sqrt{\frac{2F_{norm}\Delta}{\pi b}} \tag{4.23}$$

Any one of the contact length models can be used in this analysis by simply substituting the predicted contact length for βr_{out}.

4.3.1.2 LOAD DISTRIBUTION

The pressure distribution has an assumed elliptic shape (see Figure 4-7) with a peak pressure p_0 as described in (4.24).

$$f_{norm} = \frac{2F_{norm}}{\pi b \beta r_{out}} \tag{4.24}$$

$$\Delta = \frac{2}{\frac{1}{r_{out}} + \frac{1}{r_{wheel}}}\left[\frac{1-\nu_{wheel}^2}{E_{wheel}} + \frac{1-\nu_{cam}^2}{E_{cam}}\right] \tag{4.25}$$

r_{wheel}, E_{wheel}, ν_{wheel} are the radius, Young's modulus, and Poisson's ratio of the grinding wheel, respectively. The subscript "cam" similarly represents the cam lobe. The width of the cam face is *b*.

4.3.1.3 STRESS PROFILE

The stress profile for the normal load is determined by (4.26) to (4.30)

$$(\sigma_{\theta\theta})_{norm} = -\frac{f_{norm}}{\pi}(r_{out}-r)\left[\frac{(\beta r_{out})^2+2(r\theta)^2+2(r_{out}-r)^2}{\beta r_{out}}\overline{\Psi}-\frac{2\pi}{\beta r_{out}}-3(r\theta)\psi\right] \tag{4.26}$$

$$(\sigma_{zz})_{norm} = -\frac{f_{norm}}{\pi}(r_{out}-r)\left[\beta r_{out}\overline{\Psi}-r\theta\psi\right] \tag{4.27}$$

$$(\sigma_{r\theta})_{norm} = -\frac{f_{norm}}{\pi}(r_{out}-r)^2\psi \tag{4.28}$$

$$\psi = \frac{\pi}{K_1}\frac{1-\sqrt{\frac{K_2}{K_1}}}{\sqrt{\frac{K_2}{K_1}}\sqrt{2}\sqrt{\frac{K_2}{K_1}+\left(\frac{K_1+K_2-(2\beta r_{out})^2}{K_1}\right)}} \tag{4.29}$$

where:

$$\overline{\Psi} = \frac{\pi}{K_1}\frac{1+\sqrt{\frac{K_2}{K_1}}}{\sqrt{\frac{K_2}{K_1}}\sqrt{2}\sqrt{\frac{K_2}{K_1}+\left(\frac{K_1+K_2-(2\beta r_{out})^2}{K_1}\right)}}$$

$$K_1 = (\beta r_{out}+r\theta)^2+(r_{out}-r)^2 \tag{4.30}$$

$$K_2 = (\beta r_{out}-r\theta)^2+(r_{out}-r)^2$$

The stress profile developed by normal loads can be seen in Figure 4-8.

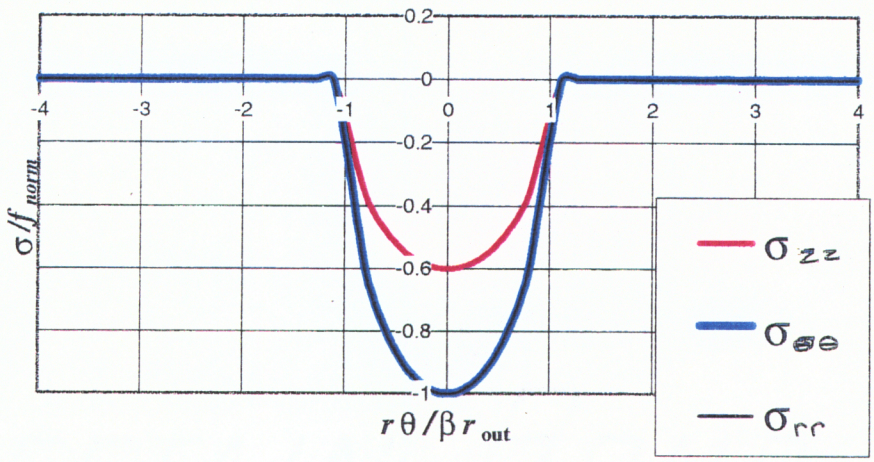

Figure 4-8 Stress profile due to normal load. Note that $\sigma_{r\theta} = 0$ on the surface for loading normal to the surface.

Note that normal pressure produces only compressive stress. We must have tensile yielding in the near-surface region in order to get the observed [Courtney, 1993, pp. 55-66], [Vansevenant, 1987, pp. 5-1 - 5-55] near-surface compressive residual stress.

4.3.2 Tangential Load

The tangential load is assumed to be proportional to the normal load. The constant of proportionality is the well-known coefficient of friction. However, the Litton-Landis grinding-machine instrumentation records both the normal and tangential force. As a result, the coefficient of friction need not be calculated, but simply assumed a constant.

4.3.2.1 Stress Profile

If we assume a constant coefficient of friction throughout the contact area the stress profile due to tangential loading only is described by (4.31) to (4.34).

$$f_{\tan} = \frac{2F_{\tan}}{\pi b \beta r_{out}} \tag{4.31}$$

$$(\sigma_{\theta\theta})_{tan} = -\frac{f_{tan}}{\pi}\left[\begin{array}{l}\left(2(\theta r)^2 - 2(\beta r_{out})^2 - 3(r_{out}-r)^2\right)\psi \\ \quad +2\pi\frac{\theta r}{\beta r_{out}} + 2\left((\beta r_{out})^2 - (\theta r)^2 - (r_{out}-r)^2\right)\frac{\theta r}{\beta r_{out}}\overline{\Psi}\end{array}\right] \tag{4.32}$$

$$(\sigma_{rr})_{tan} = -\frac{f_{tan}}{\pi}(r_{out}-r)^2\psi \tag{4.33}$$

$$(\sigma_{\theta r})_{tan} = -\frac{f_{tan}}{\pi}\left[\begin{array}{l}\left((\beta r_{out})^2 + 2(\theta r)^2 + 2(r_{out}-r)^2\right)\frac{(r_{out}-r)}{\beta r_{out}}\overline{\Psi} \\ \quad -2\pi\frac{(r_{out}-r)}{\beta r_{out}} - 3\theta r(r_{out}-r)\psi\end{array}\right] \tag{4.34}$$

The stress profile developed by the tangential loads can be seen in Figure 4-9.

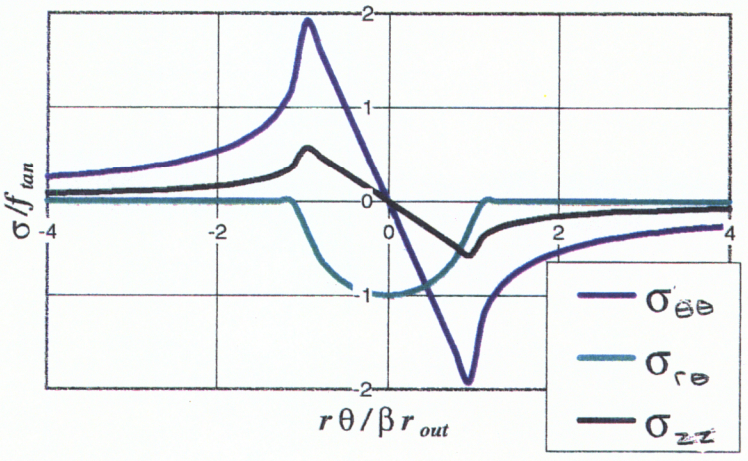

Figure 4-9 Surface stress profile due to tangential loading. Note that $\sigma_{rr} = 0$ on the surface for tangential loading

The tangential loading is interesting. Note the tensile peak at the very end of the contact area (i.e. grinding zone). This tensile peak occurs near the same position as the maximum grinding temperature, depending on the shape of the heat flux input , cooling rates, and grinding zone energy partition. Considering Figure 2-16, the material will be most likely to yield where it is hottest.

4.3.3 SUPERPOSITION OF NORMAL AND TANGENTIAL STRESSES

Using the principle of superposition we can add the tangential and normal elasticity solutions to obtain the stress profiles in Figure 4-10. The normal and tangential forces used to generate the stress profiles in Figure 4-10 were gathered at Litton-Landis during an actual grinding run.

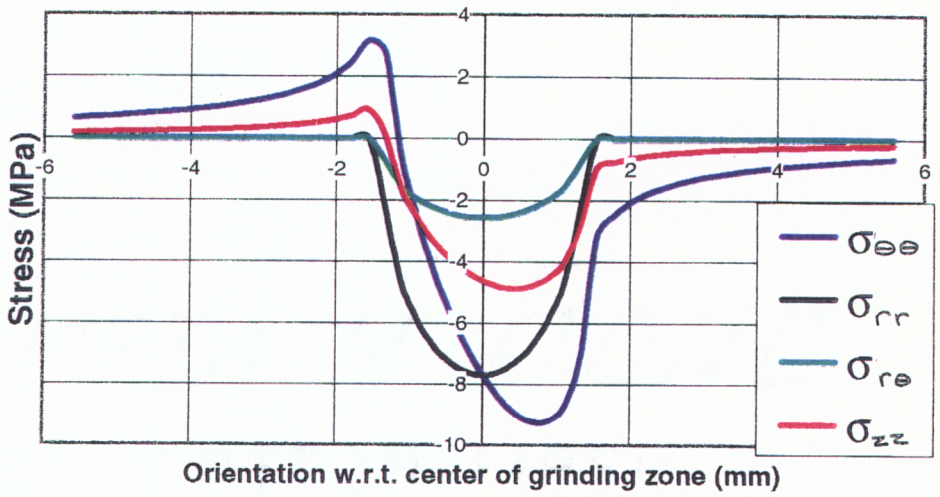

Figure 4-10 Graph of mechanical stresses generated during a sample grinding run. Note that $(\sigma_{zz} = 0)$ for plane stress.

parameters used to create the above graph:

$r_{out} = 16$ mm $\quad b = 15.8$ mm $\quad \beta = \frac{\pi}{36}$ $\quad F_{tan} = 89$ N $\quad F_{wheel} = 267$ N

The rectangular Cartesian coordinates were transformed into cylindrical coordinates for Figure 4-10 as described in Section 4.3.3.1 and dimensionalized to give an understanding of the magnitudes of the mechanical stresses.

4.3.3.1 Transformation to Polar Coordinates

The solution to the mechanical pressures as proposed has converted a problem in cylindrical coordinates to Cartesian coordinates. Therefore a choice must be made about how to return to cylindrical coordinates. No matter what choice is made, some inaccuracy will result and equilibrium is violated. However, the result will be a reasonable approximation. The Cartesian coordinates were transformed into the cylindrical coordinates in the following way:

$$z = \bar{r}_{out} - \bar{r} \tag{4.35}$$

$$x = \bar{r}\theta \tag{4.36}$$

4.3.3.2 Non-Dimensional Stress

The mechanical stress can be non-dimensionalized using the same parameters as were used for thermal stress in Section 4.2. Unfortunately, this would require the mechanical stresses to be known as specific quantities, but it also will add insight into the mechanisms acting to deform the workipiece material during grinding. If we non-dimensionalize Figure 4-10 with the parameters from equation (4.22), which are known quantities thanks to Litton-Landis's well-instrumented equipment, the result is Figure 4-11.

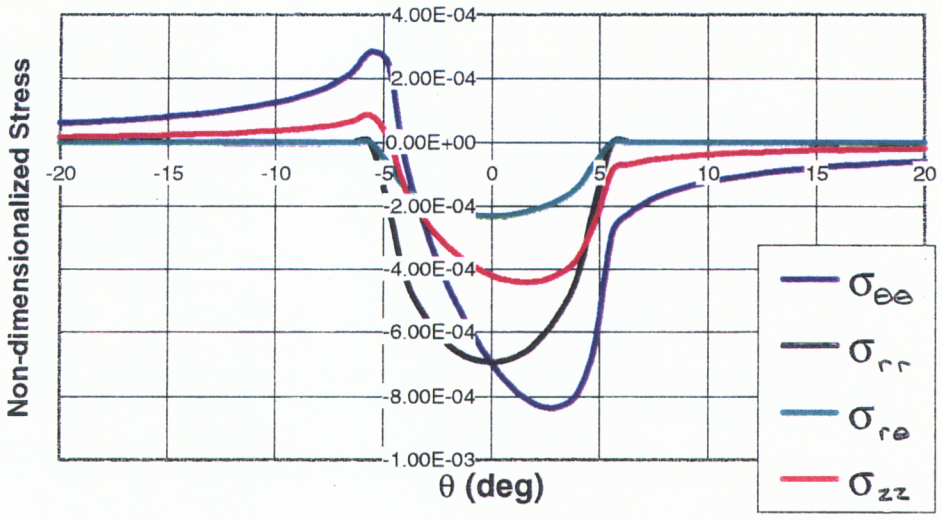

Figure 4-11 Non-dimensionalized surface mechanical stress using data from an actual grinding run. Note that $(\overline{\sigma}_{zz} = 0)$ for plane stress.

parameters used to create the above graph:

$r_{out} = 16$ mm $\qquad \beta = \frac{\pi}{36}$ $\qquad b = 15.8$ mm

$r_{wheel} = 304.8$ mm $\qquad \omega_{wheel} = 1958$ rpm $\qquad F_{tan} = 89$ N $\qquad F_{norm} = 267$ N

Comparing Figure 4-11 with Figure 4-3 and Figure 4-4, it is apparent that the mechanical stress is at least an order of magnitude less than the thermal stress when elasticity theory is used. Therefore, we have determined that mechanical stress is a secondary effect in this analysis and it will be neglected.

5. RESIDUAL STRESS PROFILES AFTER GRINDING

"... thought is impossible without an image." -Aristotle, conclusion in his treatise, On the Soul, 325 B.C.*

In this section, plasticity corrections are applied to the elastic stresses developed during grinding as developed in Section 4. As mentioned before, the plasticity corrections account for the dissipative term (2.14) that is neglected when performing an elasticity analysis. It is assumed that the depth of cut is sufficiently large so that the material which was plastically deformed by the previous pass is completely removed. Considering the depth of cut is typically 0.03 millimeters to 0.1 millimeters, this assumption should be valid.

5.1 TEMPERATURE DEPENDENT RAMBERG-OSGOOD STRESS STRAIN CURVES

Assuming each of the terms are temperature dependent The Ramberg-Osgood equation (2.35) has the following form:

$$\varepsilon(T) = \frac{\sigma(T)}{E(T)} + \left(\frac{\sigma(T)}{H(T)}\right)^{1/n(T)} \tag{5.1}$$

$$E(T) = \left[-6\cdot 10^{-5}\frac{T^2}{{}^{o}C^2} - 0.0359\frac{T}{{}^{o}C} + 210.52\right] \text{GPa} \tag{5.2}$$

Since Young's modulus as a function of temperature (5.2) has already been experimentally determined (see Figure 2-14), it only remains to find the strain hardening exponent, n, and H as a function of temperature.

---

* Aristotle (384 - 322 B.C.): Greek philosopher.

5.1.1 TEMPERATURE DEPENDENT STRAIN HARDENING EXPONENT

It has been shown that the strain hardening exponent is approximately constant with respect to temperature for at least one steel (see Figure 5-1) [Dowling, 1993, Fig. 6].

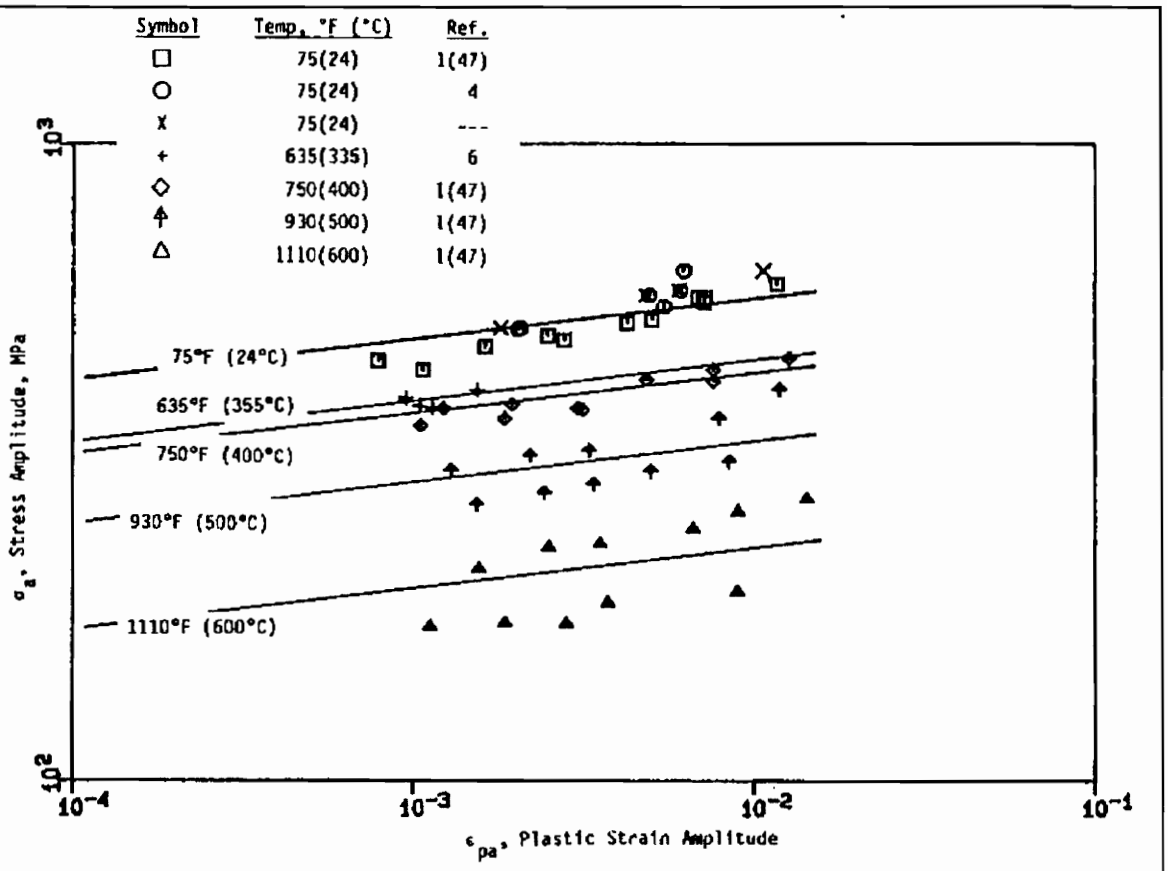

Figure 5-1 Stress amplitude vs. plastic strain amplitude for 403 SS at various temperatures [Dowling, 1985, Fig. 6]

Therefore, the strain hardening exponent for SAE 52100 steel will be assumed independent of temperature in this analysis. The strain hardening exponent for SAE 52100 has been experimentally determined to be 0.031 at 23 °C [ASM, 1985]. This means:

$$n(T) = n = 0.031 \tag{5.3}$$

5.1.2 TEMPERATURE DEPENDENT H

The temperature dependence of the Ramberg-Osgood constant, H, is determined by setting the plastic strain component of the Ramberg-Osgood equation (2.35) equal to 0.2% strain.

$$\left(\frac{\sigma_0(T)}{H(T)}\right)^{1/n(T)} = 0.002 \tag{5.4}$$

The temperature dependent yield stress (5.5) was substituted for stress (see Figure 2-16).

$$\sigma_0(T) = \left[1735 - 1.985\frac{T}{^oC} + 5.754\cdot 10^{-4}\frac{T^2}{^oC^2}\right] \text{MPa} \tag{5.5}$$

Substituting (5.3) and (5.5) into (5.4) and rearranging, we get:

$$H(T) = \frac{\sigma_o(T)}{0.002^{0.031}} \tag{5.6}$$

which can be seen graphically in Figure 5-2.

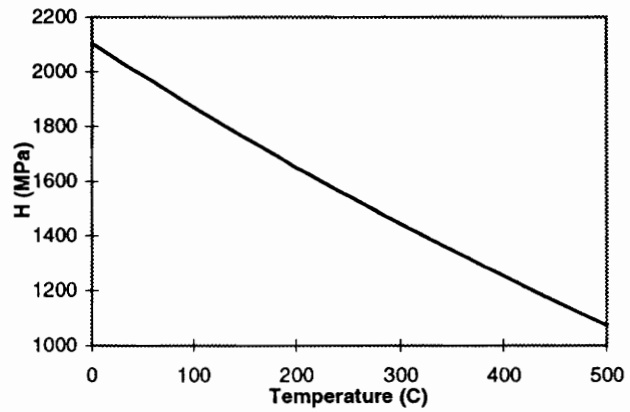

Figure 5-2. Temperature dependent Ramberg-Osgood constant, H, for SAE 52100 steel.

5.1.3 TEMPERATURE DEPENDENT RAMBERG-OSGOOD STRESS-STRAIN "SURFACE"

If the equations (5.1) - (5.6) are combined, the result is a temperature dependent Ramberg-Osgood description of the material behavior.

$$\varepsilon(T) = \frac{\sigma(T)}{\left[-6\cdot10^{-5}\frac{T^2}{{}^{o}C^2} - 0.0359\frac{T}{{}^{o}C} + 210.52\right]\text{GPa}} + 0.002\cdot\left(\frac{\sigma(T)}{\left[1735 - 1.985\frac{T}{{}^{o}C} + 5.754\cdot10^{-4}\frac{T^2}{{}^{o}C^2}\right]\text{MPa}}\right)^{\frac{1}{0.031}} \tag{5.7}$$

Equation (5.7) can be represented graphically with a three-dimensional plot (see Figure 5-3).

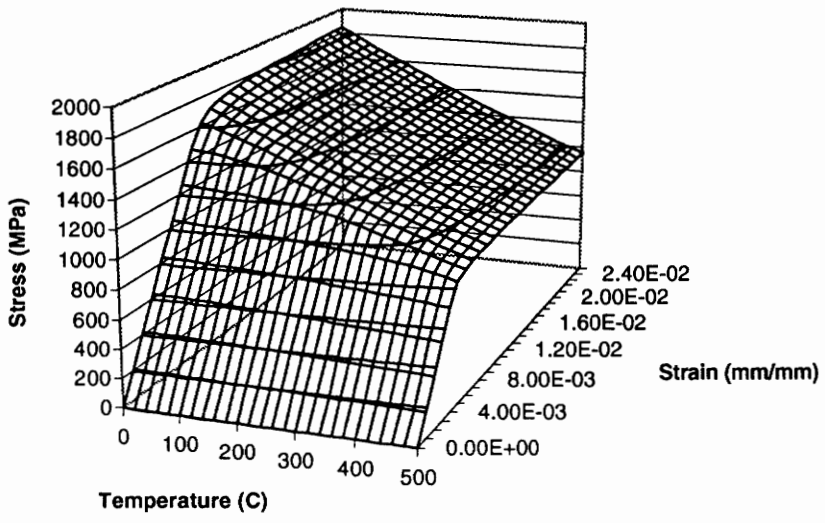

Figure 5-3. Temperature dependent Ramberg-Osgood stress-strain "surface" for SAE 52100 steel

5.2 PLASTICITY CORRECTIONS

The elastic stress profile for hoop stress can be obtained by estimating points on the non-dimensionalized stress plot (see Figure 4-3). Then these points can be given units using Eq. 4.22. Intermediate points can then be interpolated by fitting a polynomial to the known elastic points (see Figure 5-1).

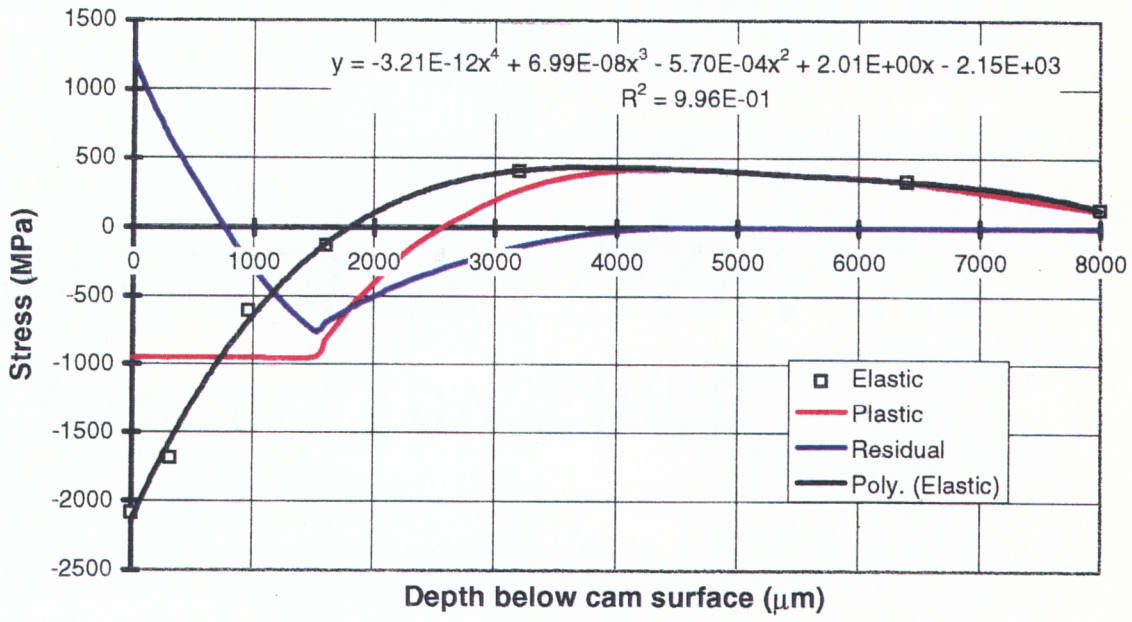

Figure 5-4 Estimated elastic, plastic, and residual stress profiles for the base circle of shaft V-8, lobe 2.

parameters used to create the above graph (see Figure 3-4 for additional parameters):

$r_{out} = 16$ mm $\quad b = 15.8$ mm $\quad \beta = \frac{\pi}{36}$ $\quad E_{cam} = 213.5$GPa $\quad \nu_{cam} = 0.3$

$k_{cam} = 30.5\frac{\text{Watt}}{\text{m}\cdot\text{K}}$ $\quad \alpha_{th} = 1.25\cdot 10^{-5}\frac{1}{\text{K}}$ $\quad \kappa_{cam} = \frac{\rho_{cam}\tilde{c}_{cam}}{k_{cam}} = 18.8\frac{\text{m}^2}{\text{sec}}$ $\quad F_{tan} = 89$ N

$Q_0 = 0.68\frac{F_{tan}\omega_{wheel}r_{wheel}}{2\beta r_{out}b}$ $\quad F_{norm} = 267$ N $\quad \omega_{wheel} = 1958$ rpm $\quad r_{wheel} = 304.8$ mm

By applying Neuber's rule as developed in Section 2.2.2 to obtain the sustainable stress at a given temperature (see Figure 5-3), and estimating the plastic zone size as twice the distance where the elastic stress crosses the sustainable stress (see Figure 2-19), the residual stress profile can be estimated in-depth (see Figure 5-4). The elastic stress profile is subtracted from the plastic stress profile to obtain the residual stress as described in section 2.2 (see Figure 2-5).

These are admittedly rough estimates. The area in tension and compression should be equal for the residual stress curve to satisfy equilibrium. Further refinement would require a more sophisticated elasto-plastic analysis.

6. DISCUSSION

The preceding sections illustrated a method for approximating the residual stress state of a finished cam. The residual stresses were assumed to be induced by the mechanical pressures and thermal stresses generated during grinding. The complex shape of the cam was reduced to a cylinder of the same radius as the local radius of curvature. In this section, insight is given to the various aspects of the problem.

By combining the thermal analysis and temperature dependent properties, useful knowledge is gained about what is happening to the material. Depending on the boundary conditions, higher temperatures could occur more towards the middle of the grinding zone. Furthermore, the material could be hotter in the subsurface than on the surface towards the end of the grinding zone.

In light of the last statement, the thermal stress could become less compressive, possibly tensile, at the point where the subsurface is the hottest point. Although the mechanical stress has been determined to be a secondary effect, the extra tensile pull it supplies at the end of the grinding zone could be just enough for tensile yielding. Rather than the simple loading and unloading analysis, one needs to perform an analysis that takes into account this loading in the opposite direction in order to see what has been found experimentally.

6.1 Comparison of Previous Results

The results are qualitatively consistent with those of previous researchers (compare Figure 6-1 and Figure 6-2). The stress profile is tensile at the surface, dying out exponentially and eventually going compressive (not shown because depth is prohibitive).

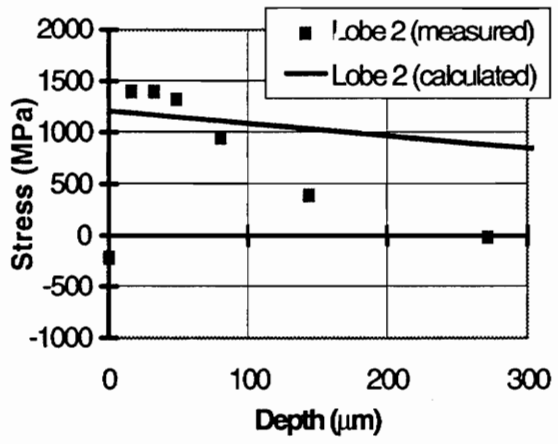

Figure 6-1 Measured [Courtney, 1993, p. 59] and calculated residual stress profiles in the base circle of various lobes of shaft V-8

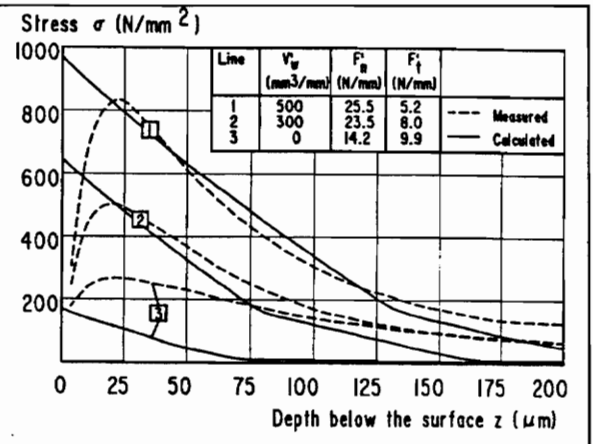

Figure 6-2 Measured and calculated residual stress profiles for surface peripheral plunge grinding with different metal removal rates [Vansevenant, 1987, p. 6-5]

The case calculated in Figure 6-1 was for just less than one complete pass. It should be understood that the cam evaluated in Figure 6-1 was subjected to six passes. This means that the elastic stress profile in Figure 4-3 and Figure 4-4 is less radical than it would be on the sixth pass, since more of the heat input to the cam would be convected away at the surface when the piece is hotter.

The experimental data in Figure 6-1 are x-ray residual stress measurements made after removing material in stages. No correction was made for redistribution of stress as this was considered negligible. Additional data is available in Courtney (1993) and Biggi (1995). Biggi analyzed cylinders using the previously described characteristic cylinder approach to see if there was a correlation between the cylinders and the actual cams tested by Courtney. Biggi found as the radius of the cylinder increased, the depth of the residual stress peak went deeper. The author attributes this effect to the increased mass of the cylinder. Increasing the radius of the cylinder examined is synonymous with increasing the cooling on the inner surface of a smaller cylinder.

6.2 Reasons for Near Surface Inconsistencies

In this study it was hoped that the magnitude of the mechanical stresses were significant enough to induce the observed near-surface compressive residual stress. However, the surface pressures were found to be inconsequential compared to the thermal stresses.

6.2.1 Shape of Heat Flux

The author now asserts that the near-surface residual stress must be a thermal phenomenon. In this analysis, the heat flux was assumed to be constant throughout the grinding zone, i.e. $q(\theta) = 1$. Numerical calculations [Cooper, 1995] and experimental evidence [Vansevenant, 1987, 3-1 - 3-58] has shown that the heat flux is best represented as a triangular distribution.

Numerical calculations of the energy partition have indicated that for certain grinding configurations there can actually be a local heat flux out of the workpiece towards the end of the grinding zone.* This phenomenon could be especially pronounced during upgrinding since the fluid is introduced at the end of the grinding zone. Assuming this is true, the thermal stress would become less compressive, possibly tensile. With help from the mechanical tensile peak at the end of the grinding zone (see Figure 4-10), the surface of the workpiece could yield in tension. This would explain the near-surface compressive residual stress which has eluded previous researchers.

---

* Telephone conversation with Professor Adrienne Lavine, UCLA, 6/2/95

7. CONCLUSIONS

Based on the results of this study of cylindrical grinding, the following conclusions can be drawn:

- Surface residual stresses were similar to those estimated based on a characteristic cylinder matching to local radius of curvature. However, the subsurface distributions do not agree very well with the crude estimate made. The cylinder approximation could be a factor here.
- The mechanical pressures of the grinding wheel create stresses at least an order of magnitude less than thermal stresses. Therefore, mechanical stresses are a secondary effect and should only be accounted for when the analysis is exact enough to warrant their consideration.
- The residual stress can be estimated by approximate plasticity corrections. However, the directionality of the dissapative stress tensor is lost. If it is necessary to maintain directionality, a more detailed plasticity analysis is necessary.
- The residual stress profile can be influenced by either heating or cooling the inside of the hollow, Presta camshafts. The stress profile can be drawn deeper by cooling the inside of the shaft, or pushed shallower by heating the inside of the shaft. Care must be taken to avoid adverse metallographic changes if the inside of the shaft is heated.

7.1 RECOMMENDATIONS

Recommendations for future work are as follows:

- A complete numerical implementation of the equations representing the stress and temperature profiles during grinding should be developed. The results could

be better interpreted by an in-depth graphical representation on a commercially available package, such as PV Wave by Visual Numerics. On a cylindrical plot the r and θ directions could represent r and θ in the characteristic cylinder, while the z axis could represent elastic stress magnitude. Temperature could also be included in this single, intuitive graph by plotting it as a color at the given stress magnitude. This graph summarizes the entire grinding process and quickly indicates changes in processes that could potentially increase output while maintaining quality.

- Cooling in the grinding zone specific to upgrinding should be investigated more closely. Due to the compressive residual stress and relative magnitudes of thermal and mechanical stresses, the author believes the magnitude of the cooling coefficient or the shape of the heat flux has been misrepresented in the past.

- An analysis of the cooling process after grinding should be performed. There are two reasons for this. First, if the average temperature of the workpiece is significant and the cooling rate fast enough, near-surface compressive residual stresses could result from the cooling that occurs after the grinding process. Second, if the post-grinding cooling rate is not fast enough to introduce near-surface compressive residual stresses, maybe they can be induced via faster cooling after grinding. Monitoring the post-grinding cooling rate might allow for increased metal removal rates while maintaining favorable residual stress states. References previously cited [Boley, 1985, pp. 549-569] have performed this type of analysis on cylinders for more extreme cases. However, their analysis can be adapted to suit cooling after grinding.

8. REFERENCES

[Aerens, 1983] Aerens, R. (1983). La determination de la longuer d'arc de contact meule-piece. *CRIF-WTCM internal report.* **1**(83).

[ASM, 1985] ASM. (1985). *Metals handbook.* (Boyer, Howard E. & Gall, Timothy L., Eds.) Metals Park, OH

[Biggi, 1995] Biggi, Brian J. (1995, April). *The effect of grinding protocol on the resultant residual stress state in cam lobes.* Senior Project. Virginia Polytechnic Institute.

[Boley, 1985] Boley, Bruno A. & Weiner, Jerome H. (1985). *Theory of thermal stresses.* Malabar, FL: Krieger publishing Co.

[Brahtz, 1955] Brahtz, J.F., & Dean, A. (1955). An account of research information pertaining to aerodynamic heating of airframes. *W.D.A.C. Tech. Rep.* in 5 volumes., pp. 55-99

[Brandin, 1978] Brandin, H. (1978). *Pendelschleifen und tiefschleifen vergleichende untersuchungen beim schleifen von rechteckprofilen.* Ph.D. Dissertation. Technical University of Braunschweig.

[Brown, 1971] Brown, R., Saito, K., & Shaw, M. (1971). Local elastic deflections in grinding. *Annals of the CIRP,* **19**, pp. 105-113.

[Chandrasekharaiah, 1986] Chandrasekharaiah, D.S. (1986). Thermoelasticity with second sound: A review. *Appl. Mech. Rev.* **39**, p. 3.

[Cooper, 1995] Cooper, William. (1995, August). *Kinematics and thermal modelling of industrial camshaft grinding.* Ph.D. Dissertation. University of California at Los Angeles.

[Courtney, 1993] Courtney, S.B. (1993, December). *A rapid non-destructive test to detect camshaft lobe grinding burn.* Master of Science Thesis. Virginia Polytechnic Institute.

[De Witt, 1990] De Witt, D.P. & Incropera, F.P. (1990). *Fundamentals of heat and mass transfer.* (3rd. ed.). New York: John Wiley & Sons.

[Dowling, 1985] Dowling, N.E. & Dunn, D.O. (1985, November). *Fatigue properties of turbine blading alloys.* Blacksburg, VA: Virginia Polytechnic Institute. Report No. VPI-E-85-6.

[Dowling, 1993] Dowling, N.E. (1993). *Mechanical behavior of materials.* New Jersey: Prentice Hall, Inc.

[Egshy, 1967] Egshy, S. (1967, May). Thermal aspects of the abrasive cutoff operation. part 1 - theoretical analysis. *Transactions of the ASME - Journal of Engineering for Industry,* pp. 356-360.

[El-Helieby, 1980] El-Helieby & Rowe, G.W. (1980). A quantitative comparison between residual stresses and fatigue properties of surface-ground bearing steel (En 31). *Wear.* **58**, pp. 155-172.

[Farkas, 1983] Farkas, I. & Szekeres, A. (1983, September 20). *Application of the modified law of heat conduction and state equation to dynamical problems of thermoelasticity.* Technical paper presented by Prof. Dr. Gy Beda. H-1521 Budapest: Department of Technical Mechanics, Technical University of Budpest.

[Flavenot, 1986] Flavenot, J.F. (1986). Effect of grinding conditions on fatigue behavior of 42cd4 grade steel. Fatigue strength estimation incorporating residual stresses using different fatigue criteria. *Residual Stresses in Science and Technology*, **2.**

[Flinn, 1990] Flinn, R.A. & Trojan, P.K. (1990). *Engineering materials and their applications*, (4th. ed.). Princeton, NJ: Houghton Mifflin Company.

[Frederick, 1965] Frederick, D. & Chang, T.S. (1965). *Continuum mechanics*, Cambridge, MA: Scientific Publishers

[Girardin, 1994] Girardin, B. (1994, June). *Contact stress analysis and fatigue life prediction for a cam-roller follower system.* Master of Science Thesis. Virginia Polytechnic Institute.

[Glinka, 1985] Glinka, G. (1985). Calculation of inelastic notch-tip strain-stress histories under cyclic loading. *Engineering Fracture Mechanics* **22**(5), pp. 839-854.

[Hahn, 1976] Hahn, R. (1976). On the loss of surface integrity and surface form due to thermoplastic stress in plunge grinding operations. *Annals of the CIRP.* **25**(1), pp. 203-207.

[Hahn, 1967] Hahn, R., & Lindsay, R. (1967). On the effect of real area of contact and normal stresses in grinding. *Annals of the CIRP.* **15**, pp. 194-204.

[Hertz, 1881] Hertz, H.R. (1881). *J. Reine angew. math.* (Crelle's J.). **92**, pp. 156-171 or Hertz, H.R. (1896). *Miscellaneous papers.* London: Jones and Schott, pp. 146-162.

[Hetnarski, 1969] Hetnarski, R.B. (1969). Stresses in long cylinder due to rotating line source of heat. *AIAA Journal.* **7**, pp. 419-423.

[Hugnell, n.d.] Hugnell, Anders & Anderson, Soren (n.d.). *Simulating follower wear in a cam-follower contact* S-100 44 Stockholm, Sweden: Machine elements, Deptartment of Machine Design. The Royal Institute of Technology.

[Jaeger, 1942] Jaeger, J.C. (1942). Moving sources of heat and the temperature at sliding contacts. *Proc. R. Soc. N.S.W.* **76**, pp. 203-224.

[Juvinall, 1967] Juvinall, R.C. (1967). *Stress, strain and strength.* New York: McGraw-Hill, pp. 370-397.

[Landgraf, 1988] Landgraf, R.W. & Chernenkoff R.A. (1988). Residual stress effects in fatigue. *Residual Stress effects on fatigue of surface processed steels.* (Champoux, R.L.; Underwood, J.H. & Kapp, J.A., Eds.). Philadelphia: ASTM, pp. 1-12.

[Lavine, 1991] Lavine, A.S. & Jen, T.-C. (1991). Thermal aspects of grinding: heat transfer to workpiece, wheel, and fluid. *Int. J. Heat Mass Transfer.* **34**(45), pp. 983-992.

[Lindsay, n.d.] Lindsay, R. & Hahn, R. (n.d.). *On the basic relationships between grinding parameters.* Worcester, MA: The Heald Machine Company - internal report.

[Lindsay, 1967] Lindsay, R. & Hahn, R. (1967). On the Effect of the Real Area of Contact and Normal Stresses in Grinding. *Annals of the CIRP.* **15**, pp. 197-204.

[Lindsay, 1971a] Lindsay, R. & Hahn, R. (1971). The principles of grinding. *Technical Report of the SME*, Dearborn, MI.

[Lindsay, 1971b] Lindsay, R. (1971). *On the metal removal and wheel removal parameters, surface finish, geometry and thermal damage in precision grinding* Ph.D. Dissertation, Worcester Polytechnic Institute.

[Malkin, 1984] Malkin, S. (1984). Grinding of metals: theory and application. *J. Applied Metalworking.* **3**(2), pp. 95-109.

[Maxwell, 1867] Maxwell, J.C. (1867). On the dynamic theory of gasses. *Phil. Trans. Roy. Soc. London* **157**, pp. 49-88.

[Ohishi, 1985] Ohishi, S. & Furukawa, Y. (1985). Analysis of workpiece temperature and grinding burn in creep feed grinding. *Bull. JSME.* **28** (242), pp. 1775-1781.

[Outwater, 1952] Outwater, J.O. & Shaw, M.C. (1952). Surface temperatures in grinding. *Transactions of the ASME.* **74**, pp. 73-86.

[Parker, 1994] Parker, Sybil P., ed. (1994). *Mcgraw hill dictionary of scientific and technical terms.* (5th ed.). New York: McGraw-Hill Book Company.

[Sauer, 1974] Sauer, W. & Shaw, M. (1974). The role of elastic deflections of wheel-work interface in surface grinding. *International Conference of Production Engineering*, Tokyo, pp. 645-649.

[Skalli, 1982] Skalli, N., Turbat, A.. & Flavenot, J. (1982). Prevision of thermal residual stresses in surface plunge grinding of steels. *Annals of the CIRP.* **31**(1), pp. 451-455.

[Smith, 1953] Smith J.O. & Liu, C.K. (1953, June). Stresses due to tangential and normal loads on an elastic solid with applications to some contact problems. *Journal of Applied Mechanics.* **20**, pp. 157-166.

[Snoeys, 1978] Snoeys, R., Maris, M., & Peters, J. (1978). Thermally Induced Damage in Grinding *Annals of the CIRP.* **27**(2), pp. 571-581.

[Snoeys, 1972] Snoeys, R., Peters, J. & Colding, B. (1972). Results of cooperative grinding research. *SME Technical Paper*, pp. MR72-216.

[Szekeres, 1980] Szekeres, Andras. (1980). Equation system of thermoelasticity using the modified law of thermal conductivity. *Per. Pol. Mech. Eng.* 24, p. 254.

[Takeuti, 1986] Takeuti, Y. (1986). Transient thermal stresses in rolls under a rotating partial heat source. In Richard B Hetnarski (Ed.), *Thermal Stresses.* **1**. New York: North-Holland, pp.506-511.

[Takeuti, 1980] Takeuti, Y. & Noda, N. (1980, August). An analysis of unsteady thermal stresses in rolls of ccp under a rotating heat source. *Journal of Engineering for Industry.* **102**, pp. 184-188.

[Tarkenton, 1994] Tarkenton, G.M. & Cramer, M.S. (1994). Nonlinear second sound in solids. *The American Pysical Society.* **49**, p. 17.

[Truesdell, 1984] Truesdell, C. (1984). *Rational thermodynamics.* (2nd ed.). New York: Springer-Verlag.

[Vansevenant, 1987] Vansevenant, I.R. (1987, September). *A subsurface integrity model in grinding.* Ph.D. Dissertation. Katholieke Universiteit Leuven..

[Verkerk, 1975] Verkerk, J. (1975). The real contact length in cylindrical plunge grinding. *Annals of the CIRP.* **24**(1), pp. 259-264.

[Yasui, 1983] Yasui, H. & Tsukuda, S. (1983). Influence of fluid type on wet grinding temperature. *Bull Japan Soc. Prec. Engng.* **17**(2), pp. 133-134.

VITA

Gregory Veronneau Moeller was born December 9, 1970, in Newton, Massachusetts to Ken and Winona. The next few years of his life are but a blur of names and faces in his memory as his family moved four times before his seventh birthday. Meridian, Mississippi, Atlanta, Georgia, and Columbia, South Carolina were each places where the Moeller's stopped, made friends, and moved on before returning to Massachusetts. This time the family settled in a small town near Plymouth called Kingston. Although our author enjoyed academics at times, school work was sometimes second to the numerous extracurricular activities he partook in: baseball, soccer, lacrosse, hockey, and judo. The family moved again in 1983 to Apple Valley, Minnesota. A year and a half later, Moeller entered high school. He decided it was time to focus on school work. Extracurricular activities dwindled to wrestling only for the next four years. Before beginning his senior year, the family moved yet again. This time it was to Gardner, Massachusetts; Winona's childhood stomping grounds. Moeller finished his senior year in Gardner, graduating fifth in his class.

The author began undergraduate studies at Worcester Polytechnic Institute in 1989 as an Air Force R.O.T.C. scholarship cadet. Juggling wrestling, A.F.R.O.T.C., school work and social events, the author learned he had an amazing ability to learn several chapters of information in a few days. He parted ways with the Air Force after the summer of 1991 and quit wrestling that Fall, deciding to focus on academics. Graduating from WPI with distinction and a BS in Mechanical Engineering in May 1993, the author took time off to tour the U.S. with his best friend, Chad Binkerd.

Returning to reality in August 1993, our author began his graduate studies at Virginia Tech. However, this time Moeller quickly learned study habits that had worked previously needed serious revision. After some readjustment, he quickly recovered by the second semester.

He will join the Westinghouse Electric Division's team on July 14, 1995. He will be an Engineer participating in the "Professional Development Program" and be assigned to the Oceanic Division in Annapolis, Maryland. Moeller is a certified Engineer-In-Training, a member of ASME, and a member of the Tau Beta Pi and Pi Tau Sigma honor societies.

Gregory V. Moeller